

On the simulations of aerosol pH in China using WRF-Chem (v4.0): sensitivities of aerosol pH and its temporal variations in haze episodes

Xueyin Ruan¹, Chun Zhao^{1,2,3,*}, Rahul A. Zaveri⁴, Pengzhen He⁵, Xinming Wang⁶, Jingyuan Shao⁷, Lei Geng^{1,2,3,*}

- 5 ¹School of Earth and Space Sciences, University of Science and Technology of China, Hefei 230026, Anhui, China
²CAS Center for Excellence in Comparative Planetology, University of Science and Technology of China, Hefei 230026, Anhui, China
³Frontiers Science Center for Planetary Exploration and Emerging Technologies, University of Science and Technology of China, Hefei, China
10 ⁴Atmospheric Sciences and Global Change Division, Pacific Northwest National Laboratory, Richland, WA 99352, USA
⁵School of Environment and Tourism, West Anhui University, Lu'an 237012, Anhui, China
⁶Guangzhou Institute of Geochemistry, Chinese Academy of Sciences, Guangzhou 510640, Guangdong, China
⁷Flight branch, Civil Aviation University of China, Tianjin 300300, China

Correspondence to: Lei Geng (genglei@ustc.edu.cn) and/or Chun Zhao (chunzhao@ustc.edu.cn)

- 15 **Abstract.** Aerosol pH is a fundamental property of aerosols in terms of atmospheric chemistry and its impact on air quality, climate and health. Precise estimation of aerosol pH in chemical transport models (CTMs) is critical ~~for~~ aerosol modeling and thus influencing policy development that partially relies on results from model simulations. We reported WRF-Chem simulated PM_{2.5} pH over China during a period with heavy haze episodes in Beijing, and explored the sensitivity of the modeled aerosol pH to factors including emissions of nonvolatile cations (NVCs) and NH₃, aerosol phase state assumption,
20 and heterogeneous production of sulfate. We ~~find~~ default WRF-Chem could predict spatial patterns of PM_{2.5} pH over China similar to other CTMs, but with generally lower pH values largely due to the underestimates of alkaline species (NVCs and NH₃) and the difference in thermodynamic treatments between different models. Increasing NH₃ emissions in the model would improve the modeled pH in comparison with offline thermodynamic model calculations of pH constrained by observations. In addition, we ~~find~~ that aerosol phase state assumption and heterogeneous sulfate production are important
25 in aerosol pH predictions for regions with low relative humidity (RH) and high anthropogenic SO₂ emissions, respectively. These factors should be better constrained in model simulations of aerosol pH in the future. Analysis of the modeled temporal trend of PM_{2.5} pH in Beijing over a haze episode revealed a clear decrease in pH from 5.24 ± 0.988 in clean period to 3.656 ± 0.549 in heavily polluted period. The increased acidity in more polluted conditions is largely due to the formation and accumulation of secondary species including sulfuric acid and nitric acid, even though being modified by alkaline species
30 (NVCs, NH₃). Our result suggests that NO₂ oxidation is unlikely to be important for heterogeneous sulfate production in Beijing haze as the effective pH for NO₂ oxidation of S(IV) is at higher pH of ~6.

1 Introduction

The acidity of atmospheric particles plays an essential role in various chemical and environmental processes. Acidified dust particles can largely enhance the solubility of transition metals which may act as nutrients in oceanic ecosystems (Meskhidze et al., 2003), affecting global biogeochemical nutrient cycles (Kanakidou et al., 2018). The dissolved metals can also generate reactive oxygen species, causing aerosol toxicity and adverse health effects (Fang et al., 2017). Particle acidity can strongly affect gas-particle partitioning of volatile and semi-volatile species such as NH_3 , HNO_3 , HCl (Keene et al., 2004; Guo et al., 2017a), as well as organic acids and bases (Ahrens et al., 2012). Moreover, particle acidity is linked to aerosol chemical reactivity by altering aqueous-phase reaction rates which are important for secondary aerosol formation. Both laboratory experiments (Gao et al., 2004; Surratt et al., 2007) and field studies (Rengarajan et al., 2011) have demonstrated that higher acidity could facilitate production of secondary organic aerosol (SOA) from oxidation of volatile organic compounds (VOCs) due to an acid-catalyzed mechanism. In addition, aerosol acidity ~~also~~ significantly affects reaction mechanisms and rates of heterogeneous sulfate production (Seinfeld et al., 2006). As one of the most abundant inorganic components in fine particles, sulfate is considered to be a key driver for the severe haze events in China (Cheng et al., 2016; Wang et al., 2016). Therefore, a thoughtful understanding of aerosol pH variability and its precise prediction are important to understand and quantify the formation rates and mechanisms of sulfate in Chinese haze using models, providing insights on the outbreak of the haze events.

However, ~~for nowadays~~, aerosol pH is poorly constrained due to difficulties in direct measurement techniques (Freedman et al., 2019; Keene et al., 1998). Instead, thermodynamic models, such as ISORROPIA II (Fountoukis and Nenes, 2007), Model for Simulating Aerosol Interactions and Chemistry (MOSAIC) (Zaveri et al., 2008), and Extended Aerosol Inorganics Model (E-AIM) (Clegg et al., 2003) are commonly used to calculate aerosol pH (Pye et al., 2020). These models typically predict particle deliquescence, gas-particle mass transfer, solid-liquid phase equilibrium, activity coefficients and aerosol water content (AWC) (Zaveri et al., 2008; Jia et al., 2018) under observed or modeled meteorological conditions and atmospheric chemical compositions. Some of these thermodynamic models have also been implemented in 3D chemical transport models (CTMs) for representation of aerosol processes. For example, the ISORROPIA II model is incorporated in many 3D models, such as the Goddard Earth Observing System with Chemistry model (GEOS-Chem), the Community Multiscale Air Quality Modeling System (CMAQ) and the PM-CAMx, while MOSAIC is employed in the Weather Research and Forecasting Model coupled with Chemistry (WRF-Chem) (Grell et al., 2005; Fast et al., 2006).

CTMs are useful tools to understand relevant physicochemical atmospheric processes and to formulate air quality management strategies. The reliability of particle acidity prediction in CTMs is crucial for aerosol modeling, especially for modeling of secondary aerosol formations, and therefore has implications for policy development. Vasilakos et al. (2018) demonstrated that pH bias simulated by CMAQ can induce nitrate partitioning bias and thus influences the response of $\text{PM}_{2.5}$ composition to emission changes in the model. Using GEOS-Chem model with prescribed particle pH values, Shao et al. (2019)

65 investigated the impact of particle pH on heterogeneous sulfate production and found that the model predicts different relative contributions of sulfate formation pathways to total atmospheric sulfate burden under different pH conditions. Furthermore, a recent review paper (Pye et al., 2020) highlighted the critical role of particle pH in model simulations of a variety of atmospheric chemical species and/or processes, as aerosol pH directly influences the chemical composition of aerosols as well as the reactivities of aerosol components.

70 Given the importance of aerosol acidity in secondary aerosol formation and its implications for the outbreak of Beijing haze, many studies have assessed the acidity of aerosols in northern China using CTMs or offline thermodynamic models constrained by observed gas and/or aerosol compositions (Cheng et al., 2016; Wang et al., 2016; Liu et al., 2017; Guo et al., 2017b; Song et al., 2018; Tan et al., 2018; Ding et al., 2019; Xie et al., 2020; Shao et al., 2019; Pye et al., 2020; Shi et al., 2019; Tao et al., 2020). Such models predicted a large range of aerosol pH (~3 to ~7) in northern China haze events with no
75 general consensus. For example, Cheng et al. (2016) estimated high aerosol pH between 5.4 to 6.2 over the North China Plain (NCP) using ISORROPIA II in forward (i.e., gas plus aerosol phase measurements as inputs) and reverse mode (i.e., only aerosol phase measurements as inputs), and Wang et al. (2016) estimated a near neutral aerosol pH of ~7 over Beijing using the same model with a stable state assumption. These two studies proposed that the high aerosol pH was driven by the neutralizing effect of high levels of ammonia over northern China, and as a result, NO₂ oxidation of dissolved S(IV) was
80 suggested to be the dominant heterogeneous sulfate formation pathway. However, not only the conclusion on the role of NO₂ oxidation in sulfate production (e.g.,(He et al., 2018; Shao et al., 2019)), but also the predicted aerosol pH during the haze events was challenged by later studies (Liu et al., 2017; Ding et al., 2019; Tan et al., 2018). In particular, Liu et al. (2017) and Guo et al. (2017b) argued that increasing NH₃ does not lead to ambient aerosol pH to near neutral and aerosols should be always acidic (pH = 4.2–4.5) over Beijing regardless the level of ammonia using ISORROPIA II with a metastable state
85 assumption. Furthermore, Song et al. (2018) pointed out that the high pH values estimated by ISORROPIA II in previous studies were in fact caused by code errors when the stable state assumption was applied. Song et al. (2018) further calculated aerosol pH for winter Beijing of ~4.6 and ~4 on average using ISORROPIA II and E-AIM in forward mode, respectively, similar to the results estimated by Liu et al. (2017) and Guo et al. (2017b). Tan et al. (2018) and Ding et al. (2019) also indicated similar acidic aerosols with average pH values between 3 and 4.5 in Beijing using ISORROPIA II. Moreover, Shi et al. (2019)
90 reported an observationally constrained aerosol pH of 3.4 ± 0.5 for Tianjin using ISORROPIA II. Using the GEOS-Chem model, Shao et al. (2019) estimated the mean aerosol pH was 4.3 (ranged from 3.0 to 5.4) for autumn and winter Beijing. Using the CAMQ model, Pye et al. (2020) predicted mean aerosol pH of 4.5 ± 0.8 for February Beijing, and an annual mean pH of 3.1 ± 1.5 for Tianjin, while Tao et al. (2020) found that the mean aerosol pH was 5.4 in NCP during January of 2013 by using WRF-Chem coupled with ISORROPIA II, which is higher than results from the aforementioned studies except that of
95 Cheng et al. (2016) and Wang et al. (2016).

WRF-Chem configured with MOSAIC is one of the most extensively used regional air quality models, and has provided insights on meteorological and physicochemical processes & mechanisms regarding air pollution issues in China (Huang et

al., 2014; Chen et al., 2016; Du et al., 2020; Sha et al., 2019). Pye et al. (2020) indicated that aerosol pH predicted by WRF-Chem with the MOSAIC thermodynamic scheme is in reasonable agreement with observationally constrained pH estimates over the contiguous United States. However, the performance of WRF-Chem configured with MOSAIC on aerosol pH prediction in China remains rarely reported and evaluated by far. In this study, we used WRF-Chem configured with MOSAIC to investigate aerosol pH over China during a few haze episodes (15 October 2014 to 02 November 2014, i.e., in the preceding weeks of the Asia-Pacific Economic Cooperation summit period) when extensive observational data ~~are were~~ available. We explored the sensitivity of the modeled aerosol pH to aerosol cation composition, aerosol phase assumption/configuration, heterogeneous sulfate productions, etc., compared the modeled results with that estimated using offline ISORROPIA II constrained by observed and modeled gas-aerosol compositions, and discussed the spatiotemporal variability of the predicted aerosol pH over China during the study period. The results should provide insights into the predictability of aerosol pH using WRF-Chem and improve the understanding of aerosol pH variability in Beijing and other regions in China.

2 Methodology

2.1 Model configuration

2.1.1 The WRF-Chem model

In this study, the version (v4.0) of WRF-Chem updated by the University of Science and Technology of China (USTC version of WRF-Chem) ~~is was~~ used. Compared to the publicly released version of WRF-Chem, the USTC version includes some additional capabilities such as contribution analysis of aerosol related processes and improved turbulent mixing of aerosols (Zhao et al., 2013a; Zhao et al., 2013b; Du et al., 2020). The model configurations used in this study ~~are were~~ summarized in Table 1. The Carbon Bond Mechanism version Z (CBMZ) (Zaveri and Peters, 1999) and the Model for Simulating Aerosol Interactions and Chemistry (MOSAIC) (Zaveri et al., 2008) with eight bins ~~are were~~ used as gas-phase and aerosol chemistry modules, respectively. The Noah land surface model (Chen and Dudhia, 2001) and the Yonsei University (YSU) planetary boundary scheme (Hong et al., 2006) ~~are were~~ used to represent land surface processes and boundary layer turbulent mixing, respectively. The Rapid Radiative Transfer Model for General Circulation (RRTMG) (Iacono et al., 2008) ~~is was~~ used to calculate the longwave and shortwave radiations.

2.1.2 MOSAIC

MOSAIC is an aerosol model with sectional approach to represent aerosol size distribution. It includes treatments for simulating aerosol physical and chemical processes such as nucleation, coagulation, gas-particle partitioning and heterogeneous chemistry. The chemical species treated by MOSAIC include sulfate, nitrate, chloride, methanesulfonate,

carbonate, ammonium, sodium, calcium, mineral dust, black carbon, organic mass, and liquid water. Potassium and magnesium are represented by equivalent amounts of sodium, while other unidentified inorganic species are gathered as “other inorganic mass” (OIN). The gas-phase species comprising H₂SO₄, MSA, HNO₃, HCl, and NH₃ are capable of partitioning into the particulate phase. MOSAIC consists of three submodules pertinent to the calculation of size-resolved aerosol pH as described below.

The Multicomponent Taylor Expansion Method (MTEM) is used to estimate the mean activity coefficients of various inorganic electrolytes in multicomponent solutions based on its values in pure binary solutions of all the individual electrolytes present in the solution (Zaveri et al., 2005b). Zdanovskii-Stokes-Robinson (ZSR) mixing rule (Zdanovskii, 1948; Stokes and Robinson, 1966) is applied for calculation of aerosol water content. Most of the MTEM and ZSR parameters are derived from the comprehensive Pitzer-Simonson-Clegg (Pitzer and Simonson, 1986; Clegg et al., 1992) model at 298.15 K for self-consistency.

The Multicomponent Equilibrium Solver for Aerosols (MESA) (Zaveri et al., 2005a) uses a pseudo-transient continuation method to solve the solid-liquid phase equilibrium reactions expressed as pseudo-transient precipitation and dissolution reactions. The equilibrium solution is determined by integrating the resulting stiff nonlinear ordinary differential equations until the system reaches the steady state.

The gas-particle partitioning module ASTEM (Adaptive Step Time-split Euler Method) is coupled with the thermodynamic module MESA-MTEM to solve the mass transfer equations (Zaveri et al., 2008). To reduce the stiffness, it first separates the non-volatile from semi-volatile gases in the numerical solver. For non-volatile gases (H₂SO₄ and MSA), ASTEM analytically integrates the condensation for all size bins, while for semi-volatile gases (HNO₃, HCl and NH₃), it numerically integrates condensation and evaporation for all size bins. Since the gas-particle mass transfer rates are strongly affected by the phase state of particles, different procedures are selected in ASTEM for completely solid, completely liquid, and mixed-phase particles.

In completely liquid or mixed-phase particles, the H⁺ ion molality (mH^+) is needed for mass transfer calculations. In order to determine mH^+ , two domains, i.e., sulfate rich and poor domains, are defined by sulfate ratio, X_t .

$$X_t = \frac{C_{NH_4^+} + C_{Na^+} + 2C_{Ca^{2+}}}{C_{SULF} + 0.5C_{H_3SO_3^-}} \quad (1)$$

Where C represents specie concentration in liquid phase, and $C_{SULF} = C_{SO_4^{2-}} + C_{HSO_4^-}$. In the sulfate-rich domain (i.e., $X_t < 2$), the liquid phase tends to absorb negligible HNO₃ and HCl due to the high acidity, thereby suppressing the oscillation behavior of H⁺ concentration during numerical integration. In this case, the equilibrium mH^+ is calculated by explicitly solving the partial dissociation of the bisulfate ion together with the electroneutrality equation (Zaveri et al., 2005b). In the sulfate-poor domain (i.e., $X_t \geq 2$), the use of equilibrium mH^+ will cause oscillations in the numerical solution associated with the condensation and/or evaporation of HNO₃, HCl and NH₃. Therefore, a new concept of dynamic mH^+ was introduced, which is a function of equilibrium constants, mass transfer coefficients, and the gas and particle-phase concentrations of all the related

species (Zaveri et al., 2008). In this approach, the surface equilibrium equations and acid-base coupled condensation approximation are solved simultaneously to determine the dynamic mH^+ in each size bin.

160 2.2 pH calculation

The pH is defined as the negative logarithm of the hydrogen ion activity in an aqueous solution, following the recommendation by the International Union of Pure and Applied Chemistry (IUPAC).

$$\text{pH} = -\log_{10} a_{H^+} = -\log_{10} \gamma_{H^+} H_{aq}^+ \quad (2)$$

165 where a_{H^+} is the activity of hydrogen ion in aqueous solution on a molality basis, γ_{H^+} is the hydrogen ion activity coefficient (in this study assumed to be unity) and H_{aq}^+ is the hydrogen ion molality in particle liquid water (mole kg^{-1} , moles of H^+ ions per kg of solvent). As MOSAIC outputs size-resolved hydrogen ion molality, the pH of $\text{PM}_{2.5}$ in the model was calculated using the following equation:

$$\text{pH}_{\text{pm}_{2.5}} = \frac{\sum_i mH_i^+ \times W_i}{\sum_i W_i} \quad (3)$$

170 where mH_i^+ (mole kg^{-1}) is the hydrogen ion molality in size bin i , and W_i (kg m^{-3}) is the aerosol water content in that particular size bin. There are 6 size bins for $\text{PM}_{2.5}$.

2.3 Experimental design

In this study, simulations ~~are were~~ performed at 36 km horizontal resolution with 1389 (west-east) \times 1498 (south-north) grid cells covering the entire China as shown in Fig. S1. The simulation period ~~is was~~ from 15 October 2014 to 02 November 2014 with the first 3 days used as model spin-up. This period ~~is was~~ chosen because severe haze events occurred in Beijing and extensive observational data ~~are were~~ available to constrain the model and evaluate the results. Initial and lateral boundary conditions for meteorological variables ~~are were~~ derived from the European Centre for Medium-Range Weather Forecasts (ECMWF) reanalysis data with a $0.703^\circ \times \sim 0.702^\circ$ horizontal resolution that are updated every 6 h (ERA-Interim dataset). The modeled u and v component wind, air temperature, and water vapor mixing ratio at layers above the planetary boundary layer (PBL) are nudged towards the reanalysis data with a 6 h timescale. (Stauffer and Seaman, 1990; Seaman et al., 1995). The modeled winds at 850 hPa and temperature at 2m are compared with the ERA5 reanalysis dataset (Fig. S2), which show that the model can reproduce these basic meteorological fields with the spatial correlation coefficient of 0.98 and 0.99, respectively. The chemical initial and boundary conditions ~~are were~~ provided by a quasi-global WRF-Chem simulation configured as described in Zhao et al. (2013a). Anthropogenic emissions ~~are were~~ obtained from the Multi-resolution Emission Inventory for China (MEIC) at a $0.1^\circ \times 0.1^\circ$ horizontal resolution for the year 2015 (Li et al., 2017a; Li et al., 2017b). For emissions outside of China, the Hemispheric Transport of Air Pollution version-2 (HTAPv2) at $0.1^\circ \times 0.1^\circ$ resolution for the

year 2010 ~~is was~~ used (Janssens-Maenhout et al., 2015). The Goddard Chemistry Aerosol Radiation and Transport (GOCART) dust emission scheme (Ginoux et al., 2001) is used to simulate natural dust emission fluxes, and the emitted dust particles are distributed into MOSAIC aerosol size bins based on the physics of scale-invariant fragmentation of brittle materials derived by Kok (2011). More details about the dust emission scheme coupled with MOSAIC aerosol scheme in WRF-Chem can be found in Zhao et al. (2010; 2013a). It is worth noting that dust and OIN are treated as two separate aerosol species in the USTC version of WRF-Chem.

All experiments conducted ~~are were~~ listed in Table 2. In addition to a default WRF-Chem simulation (named as the ORIG scenario), we ~~also conducted~~ simulations to investigate the sensitivities of the modeled pH to variables including aerosol concentrations of nonvolatile cations (NVCs, such as Na^+ , K^+ , Ca^{2+} , Mg^{2+}), semi-volatile species (e.g., ammonia and chloride), as well as aerosol phase state assumptions and heterogeneous sulfate production. These sensitivity experiments ~~are were~~ named as CTL1, CTL2, CTL3, CTL3meta, CTL3het_NoIs, and CTL3het_Is, respectively.

NVCs can strongly modulate aerosol acidity (Vasilakos et al., 2018; Kakavas et al., 2021). However, the default WRF-Chem significantly underestimates ~~d~~ NVCs concentrations as compared with observations (Fig. S3a-b3a and Fig. S3b). Note Mg^{2+} and K^+ are not included in the model but regard as charge-equivalent Na^+ , therefore the simulated Na^+ is compared to the observed sum of Na^+ , K^+ and Mg^{2+} , while simulated Ca^{2+} is directly compared with observed Ca^{2+} . As seen in Fig. S3a and S3b, Ca^{2+} and Na^+ are significantly underestimated in the ORIG simulation by ~96.8% and ~97.6%, respectively, because in ORIG simulation, the only source of Ca^{2+} is scaled to dust emissions with a mass fraction of 1.2% and Na^+ is only from seasalt emissions. These results suggest missing cation emission sources in model, which could lead to an underestimation in pH. The CTL1 experiment ~~is was~~ thus conducted with modified cation speciation profiles constrained by observations. To better match the observed NVCs concentrations, we set the mass of Ca^{2+} was 7.5% of dust and 10% of OIN, Mg^{2+} was 0.8% of dust, and Na^+ and K^+ from OIN were 13% and 5%, respectively. As a result, the simulated NVCs become more consistent with the observations, with a normalized mean bias (NMB) $\leq \pm 5\%$. Note that K^+ and Mg^{2+} were converted to charge equivalent Na^+ amounts since MOSAIC does not explicitly treat K^+ and Mg^{2+} .

Ammonia is one of the most important atmospheric alkaline species, and considered as a dominant factor causing higher aerosol pH in China than in the United States (Guo et al., 2017b; Ding et al., 2019). Previous studies indicated that NH_3 may be underestimated in current bottom-up emission inventories and using the MEIC inventory underestimated NH_3 emissions by about 40% for the north China (Zhang et al., 2018; Wang et al., 2018; Kong et al., 2019). In experiment CTL2, the NH_3 emissions ~~are were~~ multiplied by 2 and the others ~~are were~~ the same as CTL1. Figure S3c indicates that the modeled Cl^- concentration is almost zero in ORIG simulation because there is only seasalt source of chloride and anthropogenic chloride emissions are not included. On top of CTL2 simulation, we ~~also conducted~~ a chloride sensitivity simulation (i.e., CTL3) with additional emissions for chloride (assuming a 15% mass contribution from OIN) by increasing chloride emissions to improve the model prediction of aerosol chloride concentrations compared with observations. Spatial distributions of emissions of NVCs, NH_3 , and Cl^- from default configuration and its corresponding sensitivity experiment can be found in Fig. S4.

220 Ambient aerosol phase state is uncertain and difficult to constrain experimentally or theoretically due to difficulties in
 obtaining the efflorescence relative humidity (RH) for multicomponent salts. In general, aerosol can be treated as in metastable
 or stable state, where metastable means the aerosol solution is supersaturated and stable means crystallization of salts could
 occur once the solution reaches saturation. In MOSAIC, a flag called “hysteresis water content” (W_{hyst}) is transported to
 determine whether the particles at a grid point are on the stable or the metastable branch of the hysteresis curve. This is the
 225 default phase state determination method in WRF-Chem. To explore the effect of phase state determinations on the predicted
 aerosol pH, on top of CTL3 we performed CTL3meta simulation in which the aerosol phase iswas fixed as metastable.

~~The last, A~~ aerosol pH can also be influenced by heterogeneous sulfate production foras which is the main acid component
 of aerosol (Tilgner et al., 2021). We incorporateed heterogeneous S(IV) oxidations in aerosol water into MOSAIC chemical
 mechanism using the same reaction parameterizations in Shao et al. (2019). The incorporated heterogeneous reactions include
 230 reactions of dissolved S(IV) with H_2O_2 , O_3 , NO_2 and O_2 catalyzed by transition metal ions (Table S1). Under this circumstance,
 we also tested the effects of ionic strength on aerosol pH prediction as it influences heterogeneous sulfate production (Cheng
 et al., 2016; Liu et al., 2020). These two additional simulations on top of CTL3 arewere named as CTL3het_NoIs and
 CTL3het_Is, with the latter explicitlysed the effects of ionic strength on H_2O_2 and TMI-catalyzed S(IV) oxidations. In
 particular, for heterogeneous S(IV) oxidations, the first-order rate constant (k , s^{-1}) for the loss of gaseous species on aerosols
 235 iswas calculated by as follows (Jacob, 2000):

$$k = \left(\frac{R_p}{D_g} + \frac{4}{\nu\gamma} \right)^{-1} S_p \quad (4)$$

where R_p is the radius of aerosol (cm), D_g is the gas-phase molecular diffusion coefficient ($\text{cm}^2 \text{s}^{-1}$), ν is the mean molecular
 speed (cm s^{-1}), γ is the uptake coefficient of SO_2 on aerosols (dimensionless), and S_p is the aerosol surface area per unit volume
 of air ($\text{cm}^2 \text{cm}^{-3}$). The parameter γ is obtained for each heterogeneous pathways using a similar method as Shao et al. (2019):

$$240 \quad \gamma = \left[\frac{1}{\alpha} + \frac{\nu}{4K^*RT\sqrt{D_a K_{chem}}} \cdot \frac{1}{f(q)} \right]^{-1} \quad (5)$$

where α is the mass accommodation coefficient (dimensionless), K^* is the effective Henry's law constant (M atm^{-1}), R is the
 universal gas constant ($\text{L atm mol}^{-1} \text{K}^{-1}$), T is air temperature (K), D_a is the aqueous phase molecular diffusion coefficient (cm^2
 s^{-1}), K_{chem} is the first-order chemical loss rate constant in the liquid phase (s^{-1}), and $f(q)$ is given by:

$$f(q) = \coth q - \frac{1}{q} \quad (6)$$

$$245 \quad q = R_p \left(\frac{k_{chem}}{D_a} \right)^{\frac{1}{2}} \quad (7)$$

2.4 Observations

The ground observations of inorganic components of $PM_{2.5}$ (SO_4^{2-} , NO_3^- , NH_4^+ , Ca^{2+} , K^+ , Na^+ , Mg^{2+} , Cl^-) as well as the observed temperature and RH data ~~are~~were obtained from the HOPE-J³A (Haze Observation Project Especially for Jing–Jin–Ji Area) field campaign located at the campus of the University of the Chinese Academy of Sciences (40.41 °N, 116.68 °E, around 20 m from the ground) which is around 60 km northeast of downtown Beijing (He et al., 2018; Yang et al., 2018; Chen et al., 2015; Zhang et al., 2017). The aerosol composition data ~~are~~were used to evaluate the model’s prediction on NVCs and ~~Cl~~, and these data along with the observed temperature and RH ~~are~~were further used as inputs to calculate $PM_{2.5}$ pH using the ISORROPIA II model (in the forward and metastable mode). As gaseous NH_3 and HNO_3 observations are not available, we use aerosol NO_3^- only as NO_3 input and estimated gaseous NH_3 values using the empirical equation $[NH_3] \text{ (nmol mol}^{-1}\text{)} = 0.34 \times [NO_3] \text{ (nmol mol}^{-1}\text{)} + 0.63$ following He et al. (2018). In order to assess the effects of uncertainties in NH_3 concentration on aerosol pH predictions, we also run ISORROPIA II with $\pm 10\%$ fluctuations in NH_3 concentration and find little changes (i.e., $+0.03$ and -0.04 pH unit) can be induced. The ISORROPIA II model results ~~are~~were treated as observational constrained $PM_{2.5}$ pH and compared with that from the WRF-Chem simulations.

3 Results

260 3.1 Spatial variability of simulated $PM_{2.5}$ pH

Figure 1 shows the spatial distribution of the WRF-Chem predicted surface $PM_{2.5}$ pH over China averaged from 18 October 2014 to 02 November 2014 under default WRF-Chem configuration and a set of sensitivity experiments as listed in Table 2. The $PM_{2.5}$ pH ~~is~~was calculated by using weighted average aerosol water content as described in Sect. 2.2. The whole area of China ~~is~~was divided into six sub-regions (Fig. 1a) including the Taklimakan Desert (TD), the Gobi Desert (GD), the Northeast Plain (NEP), the North China Plain (NCP), the Yangtze River plain (YR) and Southern China (SC) to review the spatial variability of the modeled pH.

In ORIG simulation (Fig. 1b), WRF-Chem predicts~~ed~~ $PM_{2.5}$ pH with distinct spatial patterns, spanning ~ 0 –7 pH units over China. The highest mean $PM_{2.5}$ pH is predicted over the GD (~~-4.218 ± 2.23~~) and TD (~~-5.74 ± 1.44~~), where nonvolatile cations (e.g., Ca^{2+}) from mineral dust is abundant, and the predicted pH is consistent with CMAQ and GEOS-Chem simulations of fine-mode aerosol pH (approximately 4–6) downwind of the deserts (Pye et al., 2020). Notably, the $PM_{2.5}$ pH shows a declined trend from the north towards the south, with mean pH values over NEP, NCP, YR and SC are ~~3.02~~ ~~95 ± 0.878~~ , ~~2.329 ± 0.439~~ , 1.74 ± 0.438 and 1.766 ± 0.329 , respectively. Though the spatial features of $PM_{2.5}$ pH predicted by the default WRF-Chem model are similar with those from other chemical transport models (e.g., (Shao et al., 2019; Pye et al., 2020)), WRF-Chem generally tend~~ed~~ to predict lower aerosol pH (0.8–3.6) over most regions of southern and Central China

275 compared to other studies (1.3–5). For example, WRF-Chem predicts~~ed~~ an averaged PM_{2.5} pH of ~~(2.3 ± 1.3)~~ for Beijing during the modeling period, which is 1–2 pH units lower than those reported by other studies using offline ISORROPIA II model constrained by observed aerosol and/or gas compositions (~3–4.5) for fall and winter Beijing (Tan et al., 2018; Song et al., 2018; He et al., 2018), and ~2 units lower than the GEOS-Chem predictions within the same period (Shao et al., 2019). The WRF-Chem model predicted PM_{2.5} pH of ~2.2 in Tianjing is also lower than the values reported by Shi et al. (2019) who
280 estimated the pH of PM_{2.5} in Tianjing is ~3.4 using ISORROPIA II and ~3.1 using CMAQ. For a southern city, Guangzhou, WRF-Chem predicts~~ed~~ the pH of PM_{2.5} is ~1.2 ± 1.0, lower than the estimate from Jia et al. (2018) (~2.5–2.8) but who reported values for July and used different models (ISORROPIA II, E-AIM IV and AIOMFAC).

To show the effects of the above-mentioned influencing factors on the predicted PM_{2.5} pH, the differences in PM_{2.5} pH between sensitivity runs ~~are were also~~ displayed in Fig. 2. Compared to the ORIG run, the modeled PM_{2.5} pH in the CTL1 run
285 shows a ubiquitous increase all over China owing to the increased concentrations of NVCs in PM_{2.5} (Fig. 2a). In particular, the PM_{2.5} pH changes ~~are were~~ more prominent over the NEP and NCP regions, where PM_{2.5} pH increases~~ed~~ by more than 0.9 pH units on average (Fig. S52). For regions near the deserts, i.e., GD and TD, PM_{2.5} pH ~~are were~~ increased by 0.8 and 0.7 pH units, respectively. In comparison, relatively small increases (~0.~~765~~ and ~0.~~547~~) in PM_{2.5} pH ~~are were~~ noted over YR and SC where aerosol ~~is was~~ relatively acidic in the ORIG run (Fig. S52).

290 When NH₃ emissions ~~are were~~ doubled (CTL2 scenario), the predicted PM_{2.5} pH display~~ed~~ diverse degrees of elevation (Fig. 2b), increases~~ed~~ by 0.2–0.8 for most areas of China except for TD and GD where pH stay~~ed~~ nearly constant (Fig. 2b and Fig. S52). The rise in mean PM_{2.5} pH ~~is was~~ comparable (0.3–0.4) among NEP, NCP, YR and SC. In addition, minimal values of PM_{2.5} pH show~~ed~~ slight increases (0.2–0.6) while the maximum values remain~~ed~~ almost unchanged (Fig. S5).

For the CTL3 scenario that includes~~ed~~ extra chloride emissions, the predicted PM_{2.5} pH indicat~~ed~~ negligible decreases
295 compared to CTL2 (Fig. 2c), similar to the findings of Tao et al. (2020). Due to the low sensitivity of simulated aerosol pH to Cl⁻ concentration, the result of CTL3 scenario and the potential effect of Cl⁻ is not further discussed. However, it is noteworthy that WRF-Chem underestimat~~ed~~ Cl⁻ concentrations compared to the observations (Fig. S3c). In addition, Cl⁻ is the precursor of reactive chloride species (e.g., Cl, ClNO₂, HOCl) that are important in atmospheric oxidation capacity (Wang et al., 2019; Wang et al., 2020b). For example, reactive chloride not only influences ozone and HOx concentrations, but also directly
300 participates in atmospheric nitrate and sulfate production as oxidants (Wang et al., 2019; Wang et al., 2020b). Recent studies (Gunthe et al., 2021; Chen et al., 2022) found that chloride is also important in aerosol water uptake, playing an important role in the development of severe haze events. Therefore, future research should be devoted to the development of anthropogenic and natural chloride emissions to improve the prediction.

With regard to CTL3meta scenario which specific~~ed~~ the aerosol to be in metastable state indiscriminately, significant
305 decreases (~1.2–1.8) in PM_{2.5} pH compared to CTL3 ~~are were~~ predicted over northwestern China and Tibet while the changes ~~are were~~ smaller elsewhere (Fig. 2d). In particular, -PM_{2.5} pH decrease~~ed~~ by ~1.~~987~~ for TD and ~1.13 for GD, ~~causing-reducing~~

~~aerosol pH values down~~ to 4.8 and 4.0, respectively, whereas the metastable state assumption has ~~little impacts~~ on the predicted PM_{2.5} pH in the NCP, YR and SC regions.

310 In the CTL3het_NoIs scenario, additional sulfate production (on top of CTL3) result~~ed~~ in noticeable decrease of PM_{2.5} pH over eastern and central China (Fig. 3a) where gas precursors (e.g., SO₂) from anthropogenic emissions are high (Fig. S6). The largest decrease in the predicted mean PM_{2.5} pH ~~occurred~~ in the NCP, by about 0.9 pH unit, compared with that of 0.7 pH unit in YR, 0.325 pH unit in SC and 0.247 pH unit in NEP (Fig. S52). However, PM_{2.5} pH changes ~~became~~ negligible in TD and GD, which may be attributed to their low SO₂ emissions and low abundance of AWC that limit local heterogeneous production of sulfate. PM_{2.5} pH changes in CTL3het_Is scenario display~~ed~~ spatial patterns similar to that of
315 CTL3het_NoIs scenario but with smaller degree of decreases in PM_{2.5} pH (Fig. 3b).

3.2 Temporal variation of PM_{2.5} pH in haze events

During the study period, several haze episodes occurred over Beijing and there were several complete evolution cycles of pollution level from very clean to severely polluted conditions. Over this period, time slots ~~are were~~ referred to as “clean”, “light pollution”, “moderate pollution” and “heavy pollution” days according to different levels of PM_{2.5} mass concentrations
320 of 0–75, 75–115, 115–150, and >150 μg m⁻³, respectively. To further investigate the evolution of PM_{2.5} pH during a haze cycle, time series of the predicted PM_{2.5} pH values over Beijing during the study period ~~are were~~ shown in Fig. 4. The average values and ranges of PM_{2.5} pH during the entire period, as well as the pollution levels ~~are were~~ also listed in Table S2.

All the simulation results exhibit large but similar temporal variations in PM_{2.5} pH during the study period, typically covering extreme acidic (<2) to alkaline (>7) pH levels (Fig. 4). As shown in Table S2, the largest pH range (0.64–7.63) ~~is was~~
325 predicted by the CTL3het_NoIs scenario, and the smallest pH range fluctuating between 2.109 and 7.54 ~~is was~~ found in the CTL2 scenario. The simulated pH from other scenarios ~~variesd~~ by approximately 6 pH units. The large variations of PM_{2.5} pH during haze episodes are consistent with the results from other studies. For example, He et al. (2018) utilized ISORROPIA II to estimate PM_{2.5} pH during Beijing winter haze and found a similarly large pH range of 3.4–7.6 when assuming metastable aerosol state. Gao et al. (2020) calculated aerosol pH in Tianjin using ISORROPIA II and reported that PM_{2.5} pH ranged from
330 –0.08 to 13.75, in which pH varied more severely.

~~On the other hand,~~ similar temporal patterns of PM_{2.5} pH ~~are were~~ found in all scenarios, i.e., aerosols ~~became~~ more acidic at higher PM_{2.5} levels (Fig. 4 and Table S2). During clean period, PM_{2.5} pH spans~~ned~~ a wide range, with maximum pH values above 7 and minimum pH values below 2 (for ORIG, CTL1, CTL3het_NoIs) and below 2.5 (but above 2, for CTL2, CTL3, CTL3meta, CTL3het_Is). For light pollution period, PM_{2.5} pH exhibit~~sed~~ a similar range as in the clean period, but with
335 a lower mean value. However, under moderate and heavy pollution conditions, PM_{2.5} pH ~~is was~~ concentrated in a narrow range, varying within 1.5 pH units and with the most acidic aerosols (with mean pH values mostly between 1.5 and 3). These findings are consistent with those of Ding et al. (2019), who employed ISORROPIA II to calculate PM_{2.5} pH in Beijing for four seasons and found that the highest PM_{2.5} pH appeared on clean days ranging from 2 to 7, followed by polluted and heavily polluted

days for all seasons except winter. Analysis in Gao et al. (2020) also showed that the range of pH was more confined with
340 aggravation of air pollution.

In Fig. 4, we also plotted the offline model results of $PM_{2.5}$ pH (termed as pH-obs) from ISORROPIA II (forward mode
and metastable state) constrained by observed $PM_{2.5}$ compositions, temperature and RH. ~~As gaseous NH_3 observations were
not available, so we estimated the values using an empirical equation following He et al. (2018).~~ The observed $PM_{2.5}$
compositions are were in coarse resolution (12 or 24 hours), so that the pH-obs results are were also 12 or 24 hour averages. As
345 shown in Fig. 4, pH-obs in general varies similarly to those predicted by WRF-Chem, but with higher absolute values. The
default WRF-Chem (ORIG scenario) shows the maximum deviation (up to 2.22 pH units on average) from pH-obs. With
the modifications of NVCs and NH_3 emissions, CTL2 scenario efficiently improves the discrepancies between WRF-Chem
predictions and pH-obs (the mean bias is was reduced from 2.2 pH unit to 0.62). Similar discrepancies (~0.8 pH units) are were
found under CTL3meta and CTL3het_Is scenarios. The differences between other scenarios (i.e., CTL3 and CTL3het_NoIs)
350 and pH-obs are were larger than 1.2 pH units.

In addition, the responses of the predicted $PM_{2.5}$ pH to varying influencing factors under different pollution levels differed.
When NVCs are increased, the aerosol pH increases by 0.9 on average with the largest increase occurring during clean periods.
This is likely because of the higher fraction of NVCs from primary aerosol in addition to the insufficient neutralization by acid
species due to their low concentrations from secondary formation compared to polluted periods. In contrast, when NH_3
355 emissions are doubled, the aerosol pH increase is smaller (0.4 pH units) compared to CTL1 simulation, which can be explained
by the higher original pH and the semi-volatile nature of NH_3 . With higher NH_3 emissions, the simulated pH increases more
in more polluted periods. This is because aerosol pH is lower on more polluted conditions, which promotes more NH_3 shifting
to aerosol phase to consume H^+ , leading to increases in pH. The average pH of Beijing $PM_{2.5}$ was increased by 0.9 in CTL1
run compared to ORIG run, with the largest increase (~1.4) found in clean period and smaller increases (~0.6) occurring in all
360 other pollution periods. In contrast, the predicted pH increase (~0.36) was the smallest for the clean periods when NH_3
emissions were doubled (the CTL2 scenario), followed by light pollution (~0.92), moderate pollution (~1.11) and heavy
pollution (~1.22) periods. Both increasing Cl^- emission (CTL3 scenario) and changing phase state assumption (CTL3meta
scenario) lead led to negligible effects impact on pH in Beijing among all periods. For the two additional scenarios that
incorporate heterogeneous S(IV) reactions, when considering ionic strength effects (CTL3het_Is scenario) little changes in
365 the predicted $PM_{2.5}$ pH are were seen, but more pronounced changes are were seen when ionic strength effects are were not taken
into account (CTL3het_NoIs scenario). The latter case lead led to the decreases in pH by 0.7 and 1.3 units for moderate and
heavy pollution periods, respectively, due to increased heterogeneous production of sulfate and increases by 0.3 units for clean
period. AWC generally tracks the pattern of RH, with lowest water amount appearing during clean periods. Among all
scenarios, ORIG predicts the lowest AWC. High abundance of AWC is seen in CTL3meta since metastable assumption
370 normally predicts higher amount of water. The increased concentrations of sulfate in CTL3het NoIs would enhance aerosol

water uptake, resulting in more AWC. A detailed discussion of the correlation of AWC and pH during haze cycle can be found in Sect. 4.2.

4 Discussion

Overall, the modeled PM_{2.5} pH over China by all experiments displayed a clear spatial pattern, being more acidic in Southern China while neutral in northwestern China. This spatial pattern is mainly controlled by dust emissions from the desert regions in northwestern China. In addition, the PM_{2.5} pH appeared to be the most sensitive to the abundance of alkaline species (i.e., NVCs and NH₃). ~~In addition, f~~For NCP where ~~experienced~~ severe and frequent haze events occur, PM_{2.5} pH ~~is was also~~ very sensitive to the magnitude of heterogeneous sulfate production; while for the TD and GD regions, the phase state assumption appeared to be important. In the discussions as follows, we first analyzed the sensitivity of PM_{2.5} pH to influencing factors such as: NVCs emission, NH₃ emission, and etc., and then focus on as well as the evolution of PM_{2.5} pH in a haze development cycle in Beijing.

4.1 Sensitivity of the PM_{2.5} pH spatial variability to influencing factors

4.1.1 The influence of NVCs

Aerosol composition (e.g., shifting in the relative fractions of anions versus cations) is known to influence its pH (Tao and Murphy, 2019; Lawal et al., 2018; Ding et al., 2019). NVCs are the alkaline components of aerosol which can neutralize sulfuric acid irreversibly and impact aerosol water amount through its effects on aerosol composition which regulates aerosol hygroscopicity, thereby influencing aerosol pH both directly and indirectly (Guo et al., 2018a; Vasilakos et al., 2018; Kakavas et al., 2021).

~~In the ORIG simulation, the model significantly underestimated the observed Ca²⁺ and Na⁺ concentrations in Beijing (Fig. S3a and S3b). Note Mg²⁺ and K⁺ are not included in the model but regarded as charge equivalent Na⁺, therefore the simulated Na⁺ was compared to the observed sum of Na⁺, K⁺ and Mg²⁺, while simulated Ca²⁺ was directly compared with observed Ca²⁺. As seen in Fig. S3a and S3b, Ca²⁺ and Na⁺ were significantly underestimated in the ORIG simulation by -96.8% and -97.6%, respectively, suggesting missing cation emission sources in model, which could lead to an underestimation in pH. To improve the model's performance in NVCs prediction, in the CTL1 run we modified the cation emission profile as described in Sect. 2.3. As a result, the simulated NVCs became more consistent with the observations, with a normalized mean bias (NMB) $\leq \pm 5\%$.~~

Compared to the ORIG simulation, CTL1 predicted higher PM_{2.5} pH almost everywhere with varying degrees as illustrated in Sect. 3.1. This is mainly due to the increased aerosol NVCs. However, in areas with high NVCs emissions (e.g. TD, GD; Fig. S4b), the increase in pH is not prominent (Fig. 2a) probably because in such regions the acidic species are already

400 ~~neutralized by NVCs which are alkaline.~~ In Fig. 5a, we plotted the changes in PM_{2.5} pH in response to the changed aerosol NVCs as a function of the pH values from the ORIG simulation. The data ~~are were~~ categorized in six sub-regions as indicate in Fig. 1a. As shown in Fig. 5a, the response of PM_{2.5} pH to elevated NVCs displays a saddle-shaped curve. In all, for regions (e.g., NEP) with moderate acidic aerosol (i.e., pH = ~3–4) predicted by ORIG, their pH increased the most in response to elevated NVCs, indicating a large sensitivity of the aerosol pH to NVCs. While for regions with very acidic (e.g., in SC, pH ≤

405 ~1) or nearly neutral (e.g., in the central part of GD) aerosol pH, the response to elevated NVCs ~~are were~~ minimal~~um~~. This saddle-shaped curve response can be explained as follows. For aerosols with nearly neutral pH, they already contained high abundance of alkaline species (i.e., NVCs and/or ammonium), and addition of NVCs won't change their NVCs significantly. What is more, addition of NVCs may facilitate NH₃ partitioning to the gas-phase, lowering pH. ~~Further, carbonate could play a buffer role in keeping aerosol pH values from getting too high.~~ As a result, little to no changes in pH should be expected. On

410 the other hand, for very acidic aerosols with PM_{2.5} pH < 2, the amounts of NVCs increase cannot reduce H⁺ effectively due to excessive acids which may partition more to the aerosol phase to neutralize NVCs, and thus only exert~~sed~~ a small influence on aerosol pH. While for aerosols in intermediate pH ranges, there ~~are were~~ neither sufficient acidic species to neutralize the elevated alkaline NVCs, nor enough NVCs to buffer the added amount, so that the response ~~is was~~ large. This effect ~~is was~~ the largest for aerosols with pH around 3.

415 It is also noteworthy that, in this study the modified NVCs emission profiles ~~are were~~ only constrained by observations in Beijing (located in the center of NCP) for the purpose of sensitivity test. This may be one of the reasons why the responses of PM_{2.5} pH to elevated NVCs ~~are were~~ the most in NCP and NEP which are closely located and influenced by the same dust emission sources. Nevertheless a more accurate NVCs emission inventory needs to be addressed in future model developments given the sensitivity of the modeled pH to the abundance of aerosol NVCs.

420 4.1.2 Sensitivity to NH₃ emissions

In addition to Ca²⁺ and Na⁺ (i.e., the NVCs) abundances, NH₃ is also an important alkaline component and plays essential role in aerosol pH by neutralizing acidic components (H₂SO₄ and HNO₃) to form particulate sulfate and nitrate and thus driving NH₃ towards to the particle phase (Wang et al., 2020a; Zheng et al., 2020; Zhang et al., 2021). ~~But the NH₃ emission inventory used in WRF-Chem (MEIC) was suggested to be underestimated in China (Kong et al., 2019; Li et al., 2021). Therefore, CTL2~~

425 ~~was performed to investigate the sensitivity of the modeled PM_{2.5} pH to NH₃ emissions.~~ After doubling NH₃ emissions, the response in PM_{2.5} pH ~~is was~~ not as large as that to NVCs. This is somewhat expected as in comparison with NH₃, NVCs can also neutralize acidic components but with a greater preference due to their low volatility. As a result, in regions close to the dust sources (i.e., in the northwest) or affected by dust outflows, the relatively high pH and sufficient NVCs (Fig. S4b) tend to prevent the partitioning of NH₃ to aerosols, leading to limited response in PM_{2.5} pH to NH₃ variation. As shown in Fig. 2b, in

430 TD and GD, PM_{2.5} pH ~~are were~~ increased negligibly and even somewhat decreased. While for regions with relatively low

aerosol pH (e.g., NCP, YR), more NH_3 can be partitioned to the aerosol phase to consume H^+ , increasing pH. This is clearly seen in Fig. 5b where increases in $\text{PM}_{2.5}$ pH due to elevated NH_3 emissions ~~are were~~ larger for more acidic aerosols. These results agree well with previous studies which have shown that pH responds nonlinearly to the changes in NH_3 emissions (Wang et al., 2020a; Ding et al., 2019; Liu et al., 2017).

435 4.1.3 Sensitivity to aerosol phase state assumption

In chemical transport models, the history of the phase state of atmospheric aerosols cannot be easily tracked as aerosols move and mix quickly between different grid points due to turbulent transport (Zaveri et al., 2008). For this reason, it is challenging for models to determine whether the mixed aerosols follow the efflorescence branch (i.e., metastable state) or the deliquesced branch (i.e., stable state). When aerosols with different hydration histories and phase states mix together, the resulting particles in a given size bin must all be placed either on the stable or the metastable branch of the hysteresis curve as the aerosol size distribution at a grid point is represented by a single set of size bins. In MOSAIC, the phase state of particles in different size bins can be different as the model determines whether the particles in a given size bin are on the stable or the metastable branch using the W_{hyst} parameter (Zaveri et al., 2008). In comparison, many previous studies investigated aerosol pH during Beijing haze events by assuming the aerosols are in metastable states, which is regarded as a reasonable assumption for high RH (> 50%) conditions (Liu et al., 2017; Guo et al., 2017b; Guo et al., 2018b; Ding et al., 2019). ISORROPIA II adopted in some CTMs (e.g., GEOS-Chem, CMAQ) also applies the metastable state assumption (Shao et al., 2019).

As shown in Fig. 5c and Fig. 2d, after fixing aerosol phase to metastable, the response (decrease) of the modeled $\text{PM}_{2.5}$ pH ~~is was~~ larger for regions with aerosols that ~~are were~~ less acidic, especially for GD, TD, and central Tibet. These regions ~~are were~~ also in general with low RH (Fig. 6S4). RH is known to affect AWC and thus the phase state of aerosols. Karydis et al. (2021) reported similar findings in their modeling study, that the metastable assumption caused a pH decrease (~2 pH unit on average) over the regions with low RH and high crustal species. To explore the effects of the phase states on the predicted $\text{PM}_{2.5}$ pH, we plotted the pH of aerosols in each size bin (bin 01–bin 06 with increasing particle diameters from 0.039 to 2.5 μm) from CTL3 and CTL3meta runs in Fig. 7S5. The first impression from reviewing Fig. 7S5 is that the modeled decreases in $\text{PM}_{2.5}$ pH in CTL3meta ~~are were~~ mainly caused by changes in the first four size bins. Notably, in the CTL3 run, aerosols in these bins (01–04) in GD, TD and central Tibet ~~are were~~ determined to be mostly solid (i.e., no liquid water thus no pH exists) due to low RH. But in the CTL3meta run when metastable state ~~is was~~ assumed, these aerosols ~~are were~~ calculated to have a very small amount of water (Fig. S76) and thus the pH ~~are were~~ very low. As shown in Fig. 5c, the small changes in water content could lead to a wide fluctuation in pH. We select one area (denoted by the blue box in Fig. 7) in the pH-decreasing regions to discuss the characteristics in detail. Further analyses on the components of aerosols in these size bins in that area (Table S3) ~~in TD-indicated~~ that they ~~are were~~ high in sulfate but low in NVCs, suggesting “sulfate rich” particles that are in general highly acidic (Zaveri et al., 2008).

For regions with $RH > 70\%$, little to no changes in $PM_{2.5}$ pH ~~are~~were predicted when fixing aerosol phase to metastable (Fig. 5c and Fig. 2d). This is because that when $RH > 70\%$, aerosols in all size bins may be already determined to be in metastable state by W_{hyst} in the default MOSAIC scheme. In addition, since both states predict a liquid aerosol at ambient $RH > 70\%$ which reaches the deliquescence RH for most mixed-salt aerosols, changes in pH between stable and metastable states at higher RH should be insignificant as modeled. Our modeled results are also consistent with that from previous box model and chemical transport modeling studies which found a similarly small effect of phase assumption on pH at high RH condition (Song et al., 2018; Tao et al., 2020). In all, these results demonstrate that metastable assumption ~~is~~ might be inappropriate at low RH conditions and would lead to unrealistic pH predictions. This in turn suggests the rationality and advances of MOSAIC scheme in phase state determination in WRF-Chem.

4.1.4 Sensitivity to heterogeneous sulfate production

Sulfate is the main acidic component of aerosols and thus largely determines aerosol pH (Weber et al., 2016; Tilgner et al., 2021). We implemented the heterogeneous sulfate formation pathways on aqueous aerosols in WRF-Chem in this study, and explored the effects of ionic strength on the production rates with two additional runs, i.e., CTL3het_Is and CTL3het_NoIs. Overall, after the addition of heterogeneous S(IV) oxidations, modeled sulfate concentrations increased largely over eastern and central China (Fig. 3be), and where $PM_{2.5}$ pH decreased significantly as a consequence (Fig. 3a). This is as expected because sulfate can release free H^+ . Figure 5d shows that for these regions where $PM_{2.5}$ pH has an obvious response, the decrease of pH gets larger as original pH increases. On the other hand, the effects of sulfate production on pH can be buffered by uptake of bases (e.g., ammonia) from the gas-phase (Zheng et al., 2020), which could differ by regions depending on NH_3 level. For example, relatively prominent sulfate production occurs in the south part of Jiangxi Province, whereas the corresponding decrease in pH is less obvious, which may be partially offset by the buffering effect of excess ammonia. AWC also changes in response to changes in aerosol components, which in turn affects aerosol pH. Therefore, $PM_{2.5}$ pH change in response to additional sulfate production in the system ~~is~~was in fact a result of the combination of these factors.

Notably, for the CTL3het_Is run, $PM_{2.5}$ pH changes ~~are~~were much smaller (Fig. 3cb) compared to the CTL3het_NoIs run because of a smaller amount of additional sulfate production (Fig. 3d). As reported by Liu et al. (2020), high ionic strength can largely inhibit the TMI-catalyzed reaction rate and slow it down by a factor of ~ 85 at an ionic strength of 2.8 M. Although high ionic strength would make the reaction of S(IV) with H_2O_2 faster in aerosol water (Liu et al., 2020), the modeled low H_2O_2 concentration hindered the contribution of this reaction to sulfate production despite the effects of high ionic strength. Therefore, when ionic strength ~~is~~was considered, the heterogeneous production of sulfate ~~is~~was inhibited and thus smaller decreases in pH ~~are~~were caused. Note the inclusion of heterogeneous sulfate production here ~~is~~was just used to test the sensitivity of $PM_{2.5}$ pH to variations in acidic components, but not aiming to simulate atmospheric sulfate so that we did not conduct further analyses on the model's ability to capture observed sulfate production. Recent experimental studies suggest that interfacial chemistry at aerosol surfaces rather than in the bulk solutions may also be important for ambient sulfate

formation, such as the newly proposed aerosol-phase acceleration for the Mn-catalyzed oxidation of S(IV) (Wang et al., 2021) and water-assisted interfacial reaction of NO₂ with SO₃²⁻ (Liu and Abbatt, 2021). Inclusion of these additional sulfate formation pathways would presumably increase sulfate production and lower the modeled PM_{2.5} pH further. However, large uncertainties still remain in atmospheric sulfate formation mechanisms especially for these newly proposed mechanisms, and the kinetic parameters in concentrated solutions (i.e., the surface of aerosols) also need to be accurately constrained by further investigations.

500 4.2 Driving factors of the temporal PM_{2.5} pH variation in Beijing haze

As all modeled scenarios displayed a similar temporal variation for the studied period in Beijing, here we choose the CTL3meta scenario for further discussion on the temporal evolution of PM_{2.5} pH and driving factors under different pollution levels. CTL3meta scenario is selected because this scenario shows a better agreement with observations on PM_{2.5} compositions and allows us to make a fair comparison with ISORROPIA II in which the metastable state is also assumed. Figure 4 shows that the predicted PM_{2.5} pH values are were in general lower (more acidic) at more polluted days for all WRF-Chem simulations as well as the ISORROPIA II results constrained by observed aerosol composition, temperature and RH. To reveal this trend more clearly, the corresponding pH values in Beijing under different pollution levels modeled by the CTL3meta scenario are were illustrated in the box-and-whisker plots in Fig. 86a. In addition to the WRF-Chem predictions (Fig. 86a), the offline ISORROPIA II estimates using WRF-Chem outputs (i.e., aerosol composition, temperature and RH from CTL3meta scenario, Fig. 86b) and observations (Fig. 86c) are were also displayed. Figure 86 illustrates that PM_{2.5} pH calculated by ISORROPIA II (both based on WRF-Chem simulated data or observational data) generally shows consistent patterns as WRF-Chem simulation, and the PM_{2.5} pH is was higher during relatively clean days while the lowest during heavy pollution days. Despite their similar trend, overall ISORROPIA II predicts higher absolute pH values than that of MOSAIC with 1.1, 1.0 and 1.0 pH units higher during light, moderate and heavy pollution days, respectively, possibly due to the different thermodynamic representations such as activity coefficients and solution approach (see Text S1 for more details). The multiple model average of PM_{2.5} pH in Beijing under heavy pollution events (> 150 μg m⁻³) is was 3.656 ± 0.549. These results suggest that PM_{2.5} pH in Beijing under heavy haze conditions is likely moderate acidic (pH remains below 5.0), and thus the NO₂ oxidation pathway highly unlikely dominates in heterogeneous sulfate production. As NO₂ oxidation of dissolved S(IV) only becomes effective in less acidic pH ranges (~6) (Cheng et al., 2016). Most recently, an experimental study (Liu and Abbatt, 2021) proposed a water-assisted interfacial mechanism for SO₂ oxidation by NO₂ at the aerosol surface that can maintain its atmospheric importance at a lower pH of 5. This value is nevertheless still higher than the predicted pH during the heavy haze period and thus implying an unlikely importance of NO₂ oxidation.

In addition, we noticed that the high pH values are were generally associated with high mass fractions of NVCs and low AWC, whereas low pH values are were often accompanied by low mass fractions of NVCs and high AWC (Fig. S87). This suggests the important roles of AWC and aerosol compositions in determining PM_{2.5} pH. To explore their relationship, mass

fractions of PM_{2.5} ionic species as well as AWC under different pollution levels are shown in Fig. 9S8. As the pollution deteriorates, AWC increases and the mean value reaches 88.0 μg m⁻³ during the heavy pollution period (Fig. 9S8b). What is more, NVCs have a higher proportion of 0.19 in clean period, compared to 0.06 in light pollution period, 0.04 in moderate pollution period and 0.03 in heavy pollution period (Fig. 9S8a). This is consistent with changes in PM_{2.5} pH as NVCs tend to increase pH. These results are in line with some previous studies (Ding et al., 2019; Shi et al., 2017) who have demonstrated the role of NVCs in aerosol acidity. But some other studies found NVCs have limited impacts on aerosol pH, which may be due to the relatively minor contribution of crustal ions to aerosol mass in their cases (Liu et al., 2017; Zheng et al., 2020; Zhang et al., 2021). In addition, the mass fraction of sulfate declines from clean periods (0.16) to light and moderate pollution periods (0.08) then slightly increases in heavy pollution periods (0.10). Nitrate has the predominant mass fraction, accounting for 0.49 during clean period and remaining almost constant during other periods (0.65). Sulfate and nitrate formation are apparently enhanced on more polluted conditions. This leads to the release of free H⁺ which promotes the partitioning of ammonia into the aerosol phase, neutralizing the formed acidic species and buffering the pH. This also at least in part explains why the mass fraction of ammonium increases steadily throughout the haze evolution with 0.10, 0.18, 0.20 and 0.21 for clean, light, moderate and heavy pollution periods, respectively.

Ambient RH has also been recognized as a key factor in the evolution of winter haze events (Tie et al., 2017; Sun et al., 2013) and aerosol acidity (Tao and Murphy, 2019; Battaglia et al., 2017; Ding et al., 2019; Jia et al., 2020). This can also be seen in Fig. 4 where RH is in general high on more polluted days. Here we analyzed the correlation of AWC and pH with RH. As shown in Fig. 107, AWC exponentially increases with increasing RH, with a mean value of (0.018 ± 0.006) μg m⁻³ at 20% RH and (130 ± 43) μg m⁻³ at 100% RH. In contrast, PM_{2.5} pH shows a general decreasing trend with RH. These can be explained as follows. RH is typically low at the start-up phase of haze events, under which condition NVCs from primary aerosols would be rich and gas uptake as well as secondary aerosol formation are restricted due to the limited AWC, thereby leading to higher pH (clean period). As RH elevates with the deterioration of PM_{2.5} pollution, greater amounts of AWC are formed caused by the acceleration of aerosol hygroscopic growth. AWC then serves as an efficient medium for heterogeneous reactions on the surface of aerosols, thereby substantially enhancing secondary formation of acid species (such as sulfate and nitrate) and resulting in greater acidity. The latter is also facilitated by the accumulation of reactive gas precursors as the haze event evolves under stable boundary layer conditions. Aerosol hygroscopic growth is further enhanced by a positive feedback mechanism that the production of secondary aerosol species can in turn enhance aerosol hygroscopicity and increasing AWC (Wu et al., 2018). It should be noted that more AWC could also exert a dilution effect which would dilute the H⁺, but the acid effect likely prevails over the dilution effect leading to a net drop of pH. The schematic process of temporal evolution of PM_{2.5} pH during haze cycle in Beijing is given in Fig. 11.

4.3 Comparison of PM_{2.5} pH predictions between MOSAIC and ISORROPIA II

—To further explore the potential effects of different thermodynamic models on the modeled aerosol pH differences between this study and previous studies, we also compared the MOSAIC results with those obtained from ISORROPIA II. The WRF-Chem simulated hourly chemical concentrations along with temperature and RH in Beijing from CTL3meta scenario were used as inputs to ISORROPIA II (forward mode, assuming metastable to be consistent with CTL3meta). Time series of aerosol pH (bin 01–bin 06) predicted by the two different models are given in Fig. S9. Overall, ISORROPIA II and MOSAIC predicted a similar temporal pH trend, but ISORROPIA II in general predicted higher absolute pH values than that of MOSAIC for all particles with the size less than 2.5 μm . What is more, a regression slope of 0.87 between the calculated PM_{2.5} pH by MOSAIC and ISORROPIA II was found (Fig. S10). These findings are comparable to the results reported by Pye et al. (2020) who found that with the same model inputs, a regression slope of 0.89 between the calculated pH from the box model version of MOSAIC and ISORROPIA II was obtained. Comparisons of the pH values predicted by MOSAIC and ISORROPIA in Zaveri et al. (2008) also showed a similar phenomenon that ISORROPIA tended to predict higher values under same conditions. The discrepancy between these two models may be attributed to the higher amounts of aerosol water content predicted by ISORROPIA II relative to MOSAIC, as indicated in Fig. S11, despite both models use the same phase state assumption and RH. Difference in other fundamental thermodynamic treatments, including activity coefficients, gas particle partitioning scheme and solution approach may also account for the final pH difference. Nevertheless, the exact causes of the differences in pH predicted by these two models remain to be explored.

5 Conclusion

In this study, the performance of WRF-Chem configured with MOSAIC in predicted PM_{2.5} pH over China iswas evaluated. In particular, using the model, we assessed the evolution of PM_{2.5} pH over a few haze episodes in Beijing from 18 October 2014 to 02 November. The results indicate default WRF-Chem could predict similar spatial gradient of PM_{2.5} pH across China compared to other CTMs as reported by previous studies. However, WRF-Chem in general yielded sed low pH (0.8–3.6) over most regions compared to other models (1.3–5). This is mainly due to the model underestimations of NVCs concentrations, with additional contributions from low model NH₃ emissions as well as inherent differences in thermodynamic representations. The latter iswas further assessed by comparing against the corresponding pH predictions from offline ISORROPIA II using WRF-Chem modeled aerosol composition, temperature and RH as inputs. Compared to ISORROPIA II values, pH calculated by MOSAIC is consistently lower by 0.6 units on average, despite the pH variation trend matchesed quite well.

Further, six experiments arewere conducted to investigate the response in modeled PM_{2.5} pH to varying NVCs, NH₃, phase state assumption and sulfate production over China. The model results show that pH sensitivity have substantial spatial heterogeneity. Elevated NVCs emissions caused ed ubiquitous increases in PM_{2.5} pH with higher effects in NEP and NCP regions

where original pH is in the moderate acidic range. For regions with high or low original pH, the effects from NVCs are minor. Doubling NH₃ emission also ~~lead~~ to an increase in PM_{2.5} pH over most areas of China except for TD and GD where are characterized by high aerosol pH and sufficient NVCs. The effects of phase state assumption on pH ~~are~~ found to be minor at high RH conditions but large decrease in PM_{2.5} pH can be induced at low RH conditions due to an unrealistic metastable phase state assumption. Additional formed sulfate in aerosol water ~~tend~~ to effectively decrease PM_{2.5} pH over eastern and central China in a complex manner, due to the buffering effect of semi-volatile ammonia and the accompanied AWC change.

In addition, PM_{2.5} pH evolution during haze cycles in Beijing ~~is~~ investigated. The results indicate that aerosols ~~become~~ more acidic as haze pollution accumulating, from 5.24 ± 0.988 in clean period to 3.656 ± 0.549 in heavily polluted period, due to both changes in aerosol components and meteorological conditions. Large mass fraction of NVCs ~~is~~ ~~was~~ found to be responsible for the high aerosol pH during clean periods. The elevated AWC with increasing RH during polluted periods ~~accelerate~~ secondary aerosol formation (e.g., sulfate and nitrate), ~~enhance~~ water uptake and further ~~lower~~ pH. The moderately acidic aerosols under heavy haze conditions suggest that S(IV) oxidation by NO₂ is highly unlikely to contribute significantly to sulfate production in Beijing haze.

In all, our study suggests that NVCs and NH₃ influence the predicted PM_{2.5} pH the most at least in the WRF-Chem model, but currently the model cannot predict the abundance and variations of these species especially for Ca²⁺ and Na⁺. Future research efforts need to be undertaken to better constrain NVCs and NH₃ emissions in model to improve aerosol pH predictions. ~~A priori assumption that aerosols are at either stable or metastable state in model simulations (e.g., in GEOS-Chem) maybe less accurate compared to WRF-Chem which applies a more rigorous and computationally expensive phase state determination approach, especially for aerosol pH prediction for regions with low RH. Across China both stable and metastable state of aerosols exist, thus both states should be represented in regional and global models.~~ Follow-up studies to including more accurate and up-to-date heterogeneous sulfate formation pathways in model would also be necessary. More high temporal resolved observational datasets (e.g. hourly) are needed to help evaluate and understand the detailed evolution of pH during haze episodes as well as diurnal pattern of pH. Since observationally constrained pH is limited in terms of spatial coverage, more measurements need to be devoted to the regions where observations are rare or unavailable. In addition to aerosol composition, concurrent measurements of gas species subject to phase partitioning (e.g. HNO₃ and NH₃) will provide better constraints on acidity estimates. Measurements of size-resolved aerosol composition will also be useful to further evaluate MOSAIC predictions of aerosol pH from different size bins. What is more, future measurements can also consider to monitor throughout the boundary layer (e.g. from tall towers, mountain-based sites and aircraft) in order to provide insights into the vertical distribution of aerosol pH. The last, in-situ measurement technique of aerosol pH are desired to provide an improved understanding of aerosol pH and its effect on aerosol chemistry, and recently some approaches (e.g., Raman spectroscopy method (Cui et al., 2021; Li et al., 2022)) show the potential to do so in the future. ~~The last, more high resolution observation datasets at different locations may be necessary to further evaluate MOSAIC predictions of aerosol pH.~~

Code and data availability

The release version of WRF-Chem can be downloaded from http://www2.mmm.ucar.edu/wrf/users/download/get_source.html.

620 The modified version of WRF-Chem used in this study is archived on Zenodo at <https://doi.org/10.5281/zenodo.6359417>. The ERA-Interim reanalysis data from the European Centre for Medium-Range Weather Forecasts (ECMWF) for initial and boundary conditions can be downloaded from <https://rda.ucar.edu/datasets/ds627.0/>. [The ERA5 reanalysis data can be downloaded from https://rda.ucar.edu/datasets/ds633.1/](https://rda.ucar.edu/datasets/ds633.1/).

Author contributions

625 XR, LG and CZ designed the experiments, conducted and analyzed the simulations. XR, CZ, RZ, PH, XW, JS, and LG contributed to the discussion and final version of the paper.

Competing interests

The authors declare that they have no conflict of interest.

Acknowledgements

630 This work is financial supported from the National Natural Science Foundation of China (Awards: 41822605, 41871051 and 41727901), the Fundamental Research Funds for Central Universities and the Strategic Priority Research Program of Chinese Academy of Sciences (XDB 41000000). Pengzhen He acknowledges support from Natural Science Foundation of Anhui Province (2008085QD184) and from West Anhui University (WGKQ202001007). Rahul A. Zaveri acknowledges support from the Office of Science of the U.S. Department of Energy (DOE) as part of the Atmospheric System Research program at
635 Pacific Northwest National Laboratory (PNNL). PNNL is operated for DOE by Battelle Memorial Institute under contract DE-AC06-76RLO 1830. The numerical calculations in this paper have been done on the supercomputing system in the Supercomputing Center of University of Science and Technology of China. X.Y. R is grateful to Qiuyan Du and Mingyue Xu from USTC for help in the use of the WRF-Chem model.

640

References

- Ahrens, L., Harner, T., Shoeib, M., Lane, D. A., and Murphy, J. G.: Improved Characterization of Gas-Particle Partitioning for Per- and Polyfluoroalkyl Substances in the Atmosphere Using Annular Diffusion Denuder Samplers, *Environ. Sci. Technol.*, 46, 7199-7206, <https://doi.org/10.1021/es300898s>, 2012.
- 645 Battaglia, M. A., Jr., Douglas, S., and Hennigan, C. J.: Effect of the Urban Heat Island on Aerosol pH, *Environ. Sci. Technol.*, 51, 13095-13103, <https://doi.org/10.1021/acs.est.7b02786>, 2017.
- Chen, D., Liu, Z., Fast, J., and Ban, J.: Simulations of sulfate–nitrate–ammonium (SNA) aerosols during the extreme haze events over northern China in October 2014, *Atmos. Chem. Phys.*, 16, 10707-10724, <https://doi.org/10.5194/acp-16-10707-2016>, 2016.
- 650 Chen, F., and Dudhia, J.: Coupling an Advanced Land Surface–Hydrology Model with the Penn State–NCAR MM5 Modeling System. Part I: Model Implementation and Sensitivity, *Monthly Weather Review*, 129, 569-585, [https://doi.org/10.1175/1520-0493\(2001\)129<0569:Caalsh>2.0.Co;2](https://doi.org/10.1175/1520-0493(2001)129<0569:Caalsh>2.0.Co;2), 2001.
- Chen, Y., Wang, Y., Nenes, A., Wild, O., Song, S., Hu, D., Liu, D., He, J., Hildebrandt Ruiz, L., Apte, J. S., Gunthe, S. S., and Liu, P.: Ammonium Chloride Associated Aerosol Liquid Water Enhances Haze in Delhi, India, *Environ. Sci. Technol.*, <https://doi.org/10.1021/acs.est.2c00650>, 2022.
- 655 Chen, Z., Zhang, J., Zhang, T., Liu, W., and Liu, J.: Haze observations by simultaneous lidar and WPS in Beijing before and during APEC, 2014, *Science China Chemistry*, 58, 1385-1392, <https://doi.org/10.1007/s11426-015-5467-x>, 2015.
- 660 Cheng, Y., Zheng, G., Wei, C., Mu, Q., Zheng, B., Wang, Z., Gao, M., Zhang, Q., He, K., Carmichael, G., Pöschl, U., and Su, H.: Reactive nitrogen chemistry in aerosol water as a source of sulfate during haze events in China, *Science Advances*, 2, e1601530, <https://doi.org/10.1126/sciadv.1601530>, 2016.
- Clegg, S. L., Pitzer, K. S., and Brimblecombe, P.: Thermodynamics of multicomponent, miscible, ionic solutions. Mixtures including unsymmetrical electrolytes, *J. Phys. Chem.*, 96, 9470-9479, <https://doi.org/10.1021/j100202a074>, 1992.
- 665 Clegg, S. L., Seinfeld, J. H., and Edney, E. O.: Thermodynamic modelling of aqueous aerosols containing electrolytes and dissolved organic compounds. II. An extended Zdanovskii–Stokes–Robinson approach, *J. Aerosol Sci.*, 34, 667-690, [https://doi.org/10.1016/S0021-8502\(03\)00019-3](https://doi.org/10.1016/S0021-8502(03)00019-3), 2003.
- Cui, X., Tang, M., Wang, M., and Zhu, T.: Water as a probe for pH measurement in individual particles using micro-Raman spectroscopy, *Anal. Chim. Acta*, 1186, 339089, <https://doi.org/10.1016/j.aca.2021.339089>, 2021.
- 670 Ding, J., Zhao, P., Su, J., Dong, Q., Du, X., and Zhang, Y.: Aerosol pH and its driving factors in Beijing, *Atmos. Chem. Phys.*, 19, 7939-7954, <https://doi.org/10.5194/acp-19-7939-2019>, 2019.
- Du, Q. Y., Zhao, C., Zhang, M. S., Dong, X., Chen, Y., Liu, Z., Hu, Z. Y., Zhang, Q., Li, Y. B., Yuan, R. M., and Miao, S. G.: Modeling diurnal variation of surface PM_{2.5} concentrations over East China with WRF-Chem: impacts from boundary-layer mixing and anthropogenic emission, *Atmos. Chem. Phys.*, 20, 2839-2863, <https://doi.org/10.5194/acp-20-2839-2020>, 2020.
- 675 Fang, T., Guo, H. Y., Zeng, L. H., Verma, V., Nenes, A., and Weber, R. J.: Highly Acidic Ambient Particles, Soluble Metals, and Oxidative Potential: A Link between Sulfate and Aerosol Toxicity, *Environ. Sci. Technol.*, 51, 2611-2620, <https://doi.org/10.1021/acs.est.6b06151>, 2017.
- 680

- Fast, J. D., Gustafson, W. I., Easter, R. C., Zaveri, R. A., Barnard, J. C., Chapman, E. G., Grell, G. A., and Peckham, S. E.: Evolution of ozone, particulates, and aerosol direct radiative forcing in the vicinity of Houston using a fully coupled meteorology-chemistry-aerosol model, *J. Geophys. Res.-Atmos.*, 111, D21305, <https://doi.org/10.1029/2005jd006721>, 2006.
- 685 Fountoukis, C., and Nenes, A.: ISORROPIA II: a computationally efficient thermodynamic equilibrium model for $K^+-Ca^{2+}-Mg^{2+}-NH_4^+-Na^+-SO_4^{2-}-NO_3^- -Cl^- -H_2O$ aerosols, *Atmos. Chem. Phys.*, 7, 4639-4659, <https://doi.org/10.5194/acp-7-4639-2007>, 2007.
- Freedman, M. A., Ott, E. J. E., and Marak, K. E.: Role of pH in Aerosol Processes and Measurement Challenges, *J. Phys. Chem. A*, 123, 1275-1284, <https://doi.org/10.1021/acs.jpca.8b10676>, 2019.
- 690 Gao, J., Wei, Y., Shi, G., Yu, H., Zhang, Z., Song, S., Wang, W., Liang, D., and Feng, Y.: Roles of RH, aerosol pH and sources in concentrations of secondary inorganic aerosols, during different pollution periods, *Atmos. Environ.*, 241, <https://doi.org/10.1016/j.atmosenv.2020.117770>, 2020.
- Gao, S., Ng, N. L., Keywood, M., Varutbangkul, V., Bahreini, R., Nenes, A., He, J. W., Yoo, K. Y., Beauchamp, J. L., Hodyss, R. P., Flagan, R. C., and Seinfeld, J. H.: Particle phase acidity and oligomer
695 formation in secondary organic aerosol, *Environ. Sci. Technol.*, 38, 6582-6589, <https://doi.org/10.1021/es049125k>, 2004.
- Ginoux, P., Chin, M., Tegen, I., Prospero, J. M., Holben, B., Dubovik, O., and Lin, S. J.: Sources and distributions of dust aerosols simulated with the GOCART model, *J. Geophys. Res.-Atmos.*, 106, 20255-20273, <https://doi.org/10.1029/2000JD000053>, 2001.
- 700 Grell, G. A., Peckham, S. E., Schmitz, R., McKeen, S. A., Frost, G., Skamarock, W. C., and Eder, B.: Fully coupled "online" chemistry within the WRF model, *Atmos. Environ.*, 39, 6957-6975, <https://doi.org/10.1016/j.atmosenv.2005.04.027>, 2005.
- Gunthe, S. S., Liu, P., Panda, U., Raj, S. S., Sharma, A., Darbyshire, E., Reyes-Villegas, E., Allan, J., Chen, Y., Wang, X., Song, S., Pöhlker, M. L., Shi, L., Wang, Y., Kommula, S. M., Liu, T., Ravikrishna,
705 R., McFiggans, G., Mickley, L. J., Martin, S. T., Pöschl, U., Andreae, M. O., and Coe, H.: Enhanced aerosol particle growth sustained by high continental chlorine emission in India, *Nat. Geosci.*, 14, 77-84, <https://doi.org/10.1038/s41561-020-00677-x>, 2021.
- Guo, H., Liu, J., Froyd, K. D., Roberts, J. M., Veres, P. R., Hayes, P. L., Jimenez, J. L., Nenes, A., and Weber, R. J.: Fine particle pH and gas-particle phase partitioning of inorganic species in Pasadena,
710 California, during the 2010 CalNex campaign, *Atmos. Chem. Phys.*, 17, 5703-5719, <https://doi.org/10.5194/acp-17-5703-2017>, 2017a.
- Guo, H., Weber, R. J., and Nenes, A.: High levels of ammonia do not raise fine particle pH sufficiently to yield nitrogen oxide-dominated sulfate production, *Sci. Rep.*, 7, 12109, <https://doi.org/10.1038/s41598-017-11704-0>, 2017b.
- 715 Guo, H., Nenes, A., and Weber, R. J.: The underappreciated role of nonvolatile cations in aerosol ammonium-sulfate molar ratios, *Atmos. Chem. Phys.*, 18, 17307-17323, <https://doi.org/10.5194/acp-18-17307-2018>, 2018a.
- Guo, H., Otjes, R., Schlag, P., Kiendler-Scharr, A., Nenes, A., and Weber, R. J.: Effectiveness of ammonia
720 reduction on control of fine particle nitrate, *Atmos. Chem. Phys.*, 18, 12241-12256, <https://doi.org/10.5194/acp-18-12241-2018>, 2018b.

- He, P., Alexander, B., Geng, L., Chi, X., Fan, S., Zhan, H., Kang, H., Zheng, G., Cheng, Y., Su, H., Liu, C., and Xie, Z.: Isotopic constraints on heterogeneous sulfate production in Beijing haze, *Atmos. Chem. Phys.*, 18, 5515-5528, <https://doi.org/10.5194/acp-18-5515-2018>, 2018.
- 725 Hong, S. Y., Noh, Y., and Dudhia, J.: A new vertical diffusion package with an explicit treatment of entrainment processes, *Monthly Weather Review*, 134, 2318-2341, <https://doi.org/10.1175/Mwr3199.1>, 2006.
- Huang, X., Song, Y., Zhao, C., Li, M., Zhu, T., Zhang, Q., and Zhang, X.: Pathways of sulfate enhancement by natural and anthropogenic mineral aerosols in China, *J. Geophys. Res.-Atmos.*, 119, 14,165-114,179, <https://doi.org/10.1002/2014jd022301>, 2014.
- 730 Iacono, M. J., Delamere, J. S., Mlawer, E. J., Shephard, M. W., Clough, S. A., and Collins, W. D.: Radiative forcing by long-lived greenhouse gases: Calculations with the AER radiative transfer models, *J. Geophys. Res.-Atmos.*, 113, <https://doi.org/10.1029/2008jd009944>, 2008.
- Jacob, D. J.: Heterogeneous chemistry and tropospheric ozone, *Atmos. Environ.*, 34, 2131-2159, [https://doi.org/10.1016/S1352-2310\(99\)00462-8](https://doi.org/10.1016/S1352-2310(99)00462-8), 2000.
- 735 Janssens-Maenhout, G., Crippa, M., Guizzardi, D., Dentener, F., Muntean, M., Pouliot, G., Keating, T., Zhang, Q., Kurokawa, J., Wankmuller, R., van der Gon, H. D., Kuenen, J. J. P., Klimont, Z., Frost, G., Darras, S., Koffi, B., and Li, M.: HTAP_v2.2: a mosaic of regional and global emission grid maps for 2008 and 2010 to study hemispheric transport of air pollution, *Atmos. Chem. Phys.*, 15, 11411-11432, <https://doi.org/10.5194/acp-15-11411-2015>, 2015.
- 740 Jia, S., Wang, X., Zhang, Q., Sarkar, S., Wu, L., Huang, M., Zhang, J., and Yang, L.: Technical note: Comparison and interconversion of pH based on different standard states for aerosol acidity characterization, *Atmos. Chem. Phys.*, 18, 11125-11133, <https://doi.org/10.5194/acp-18-11125-2018>, 2018.
- 745 Jia, S. G., Chen, W. H., Zhang, Q., Krishnan, P., Mao, J. Y., Zhong, B. Q., Huang, M. J., Fan, Q., Zhang, J. P., Chang, M., Yang, L. M., and Wang, X. M.: A quantitative analysis of the driving factors affecting seasonal variation of aerosol pH in Guangzhou, China, *Sci. Total Environ.*, 725, <https://doi.org/10.1016/j.scitotenv.2020.138228>, 2020.
- Kakavas, S., Patoulias, D., Zakoura, M., Nenes, A., and Pandis, S. N.: Size-resolved aerosol pH over Europe during summer, *Atmos. Chem. Phys.*, 21, 799-811, <https://doi.org/10.5194/acp-21-799-2021>, 750 2021.
- Kanakidou, M., Myriokefalitakis, S., and Tsigaridis, K.: Aerosols in atmospheric chemistry and biogeochemical cycles of nutrients, *Environ. Res. Lett.*, 13, 063004, <https://doi.org/10.1088/1748-9326/aabcdb>, 2018.
- 755 Karydis, V. A., Tsimpidi, A. P., Pozzer, A., and Lelieveld, J.: How alkaline compounds control atmospheric aerosol particle acidity, *Atmos. Chem. Phys.*, 21, 14983-15001, <https://doi.org/10.5194/acp-21-14983-2021>, 2021.
- Keene, W. C., Sander, R., Pszenny, A. A. P., Vogt, R., Crutzen, P. J., and Galloway, J. N.: Aerosol pH in the marine boundary layer: A review and model evaluation, *J. Aerosol Sci.*, 29, 339-356, [https://doi.org/10.1016/S0021-8502\(97\)10011-8](https://doi.org/10.1016/S0021-8502(97)10011-8), 1998.

- 760 Keene, W. C., Pszenny, A. A. P., Maben, J. R., Stevenson, E., and Wall, A.: Closure evaluation of size-resolved aerosol pH in the New England coastal atmosphere during summer, *J. Geophys. Res.-Atmos.*, 109, <https://doi.org/10.1029/2004jd004801>, 2004.
- Kok, J. F.: A scaling theory for the size distribution of emitted dust aerosols suggests climate models underestimate the size of the global dust cycle, *Proc. Natl. Acad. Sci. U. S. A.*, 108, 1016-1021, 765 <https://doi.org/10.1073/pnas.1014798108>, 2011.
- Kong, L., Tang, X., Zhu, J., Wang, Z., Pan, Y., Wu, H., Wu, L., Wu, Q., He, Y., Tian, S., Xie, Y., Liu, Z., Sui, W., Han, L., and Carmichael, G.: Improved Inversion of Monthly Ammonia Emissions in China Based on the Chinese Ammonia Monitoring Network and Ensemble Kalman Filter, *Environ. Sci. Technol.*, 53, 12529-12538, <https://doi.org/10.1021/acs.est.9b02701>, 2019.
- 770 Lawal, A. S., Guan, X., Liu, C., Henneman, L. R. F., Vasilakos, P., Bhogineni, V., Weber, R. J., Nenes, A., and Russell, A. G.: Linked Response of Aerosol Acidity and Ammonia to SO₂ and NO_x Emissions Reductions in the United States, *Environ. Sci. Technol.*, 52, 9861-9873, <https://doi.org/10.1021/acs.est.8b00711>, 2018.
- 775 Li, B., Chen, L., Shen, W., Jin, J., Wang, T., Wang, P., Yang, Y., and Liao, H.: Improved gridded ammonia emission inventory in China, *Atmos. Chem. Phys. Discuss.*, 2021, 1-26, <https://doi.org/10.5194/acp-2021-439>, 2021.
- Li, L.-F., Chen, Z., Liu, P., and Zhang, Y.-H.: Direct Measurement of pH Evolution in Aerosol Microdroplets Undergoing Ammonium Depletion: A Surface-Enhanced Raman Spectroscopy Approach, *Environ. Sci. Technol.*, 56, 6274-6281, <https://doi.org/10.1021/acs.est.1c08626>, 2022.
- 780 Li, M., Zhang, Q., Kurokawa, J., Woo, J. H., He, K. B., Lu, Z. F., Ohara, T., Song, Y., Streets, D. G., Carmichael, G. R., Cheng, Y. F., Hong, C. P., Huo, H., Jiang, X. J., Kang, S. C., Liu, F., Su, H., and Zheng, B.: MIX: a mosaic Asian anthropogenic emission inventory under the international collaboration framework of the MICS-Asia and HTAP, *Atmos. Chem. Phys.*, 17, 935-963, <https://doi.org/10.5194/acp-17-935-2017>, 2017a.
- 785 Li, R., Dong, X., Guo, J. C., Fu, Y. F., Zhao, C., Wang, Y., and Min, Q. L.: The implications of dust ice nuclei effect on cloud top temperature in a complex mesoscale convective system, *Scientific Reports*, 7, <https://doi.org/10.1038/s41598-017-12681-0>, 2017b.
- Liu, M., Song, Y., Zhou, T., Xu, Z., Yan, C., Zheng, M., Wu, Z., Hu, M., Wu, Y., and Zhu, T.: Fine particle pH during severe haze episodes in northern China, *Geophys. Res. Lett.*, 44, 5213-5221, 790 <https://doi.org/10.1002/2017gl073210>, 2017.
- Liu, T., Clegg, S. L., and Abbatt, J. P. D.: Fast oxidation of sulfur dioxide by hydrogen peroxide in deliquesced aerosol particles, *Proc. Natl. Acad. Sci. U. S. A.*, 117, 1354-1359, <https://doi.org/10.1073/pnas.1916401117>, 2020.
- 795 Liu, T., and Abbatt, J. P. D.: Oxidation of sulfur dioxide by nitrogen dioxide accelerated at the interface of deliquesced aerosol particles, *Nat. Chem.*, <https://doi.org/10.1038/s41557-021-00777-0>, 2021.
- Meskhidze, N., Chameides, W. L., Nenes, A., and Chen, G.: Iron mobilization in mineral dust: Can anthropogenic SO₂ emissions affect ocean productivity? , *Geophys. Res. Lett.*, 30, 2085, <https://doi.org/10.1029/2003gl018035>, 2003.
- 800 Pitzer, K. S., and Simonson, J. M.: Thermodynamics of multicomponent, miscible, ionic systems: theory and equations, *J. Phys. Chem.*, 90, 3005-3009, <https://doi.org/10.1021/j100404a042>, 1986.

- 805 Pye, H. O. T., Nenes, A., Alexander, B., Ault, A. P., Barth, M. C., Clegg, S. L., Collett, J. L., Fahey, K. M., Hennigan, C. J., Herrmann, H., Kanakidou, M., Kelly, J. T., Ku, I. T., McNeill, V. F., Riemer, N., Schaefer, T., Shi, G. L., Tilgner, A., Walker, J. T., Wang, T., Weber, R., Xing, J., Zaveri, R. A., and Zuend, A.: The acidity of atmospheric particles and clouds, *Atmos. Chem. Phys.*, 20, 4809-4888, <https://doi.org/10.5194/acp-20-4809-2020>, 2020.
- Rengarajan, R., Sudheer, A. K., and Sarin, M. M.: Aerosol acidity and secondary organic aerosol formation during wintertime over urban environment in western India, *Atmos Environ*, 45, 1940-1945, <https://doi.org/10.1016/j.atmosenv.2011.01.026>, 2011.
- 810 Seaman, N. L., Stauffer, D. R., and Lario-Gibbs, A. M.: A Multiscale Four-Dimensional Data Assimilation System Applied in the San Joaquin Valley during SARMAP. Part I: Modeling Design and Basic Performance Characteristics *J. Appl. Meteorol.*, 34, 1739-1761, [https://doi.org/10.1175/1520-0450\(1995\)034<1739:Amfdda>2.0.Co;2](https://doi.org/10.1175/1520-0450(1995)034<1739:Amfdda>2.0.Co;2), 1995.
- Seinfeld, J. H., Pandis, S. N., and Noone, K.: *Atmospheric Chemistry and Physics: From Air Pollution to Climate Change*, Wiley, 2006.
- 815 Sha, T., Ma, X., Jia, H., Tian, R., Chang, Y., Cao, F., and Zhang, Y.: Aerosol chemical component: Simulations with WRF-Chem and comparison with observations in Nanjing, *Atmos. Environ.*, 218, <https://doi.org/10.1016/j.atmosenv.2019.116982>, 2019.
- 820 Shao, J. Y., Chen, Q. J., Wang, Y. X., Lu, X., He, P. Z., Sun, Y. L., Shah, V., Martin, R. V., Philip, S., Song, S. J., Zhao, Y., Xie, Z. Q., Zhang, L., and Alexander, B.: Heterogeneous sulfate aerosol formation mechanisms during wintertime Chinese haze events: air quality model assessment using observations of sulfate oxygen isotopes in Beijing, *Atmos. Chem. Phys.*, 19, 6107-6123, <https://doi.org/10.5194/acp-19-6107-2019>, 2019.
- 825 Shi, G., Xu, J., Peng, X., Xiao, Z., Chen, K., Tian, Y., Guan, X., Feng, Y., Yu, H., Nenes, A., and Russell, A. G.: pH of Aerosols in a Polluted Atmosphere: Source Contributions to Highly Acidic Aerosol, *Environ. Sci. Technol.*, 51, 4289-4296, <https://doi.org/10.1021/acs.est.6b05736>, 2017.
- Shi, X. R., Nenes, A., Xiao, Z. M., Song, S. J., Yu, H. F., Shi, G. L., Zhao, Q. Y., Chen, K., Feng, Y. C., and Russell, A. G.: High-Resolution Data Sets Unravel the Effects of Sources and Meteorological Conditions on Nitrate and Its Gas-Particle Partitioning, *Environ. Sci. Technol.*, 53, 3048-3057, <https://doi.org/10.1021/acs.est.8b06524>, 2019.
- 830 Song, S., Gao, M., Xu, W., Shao, J., Shi, G., Wang, S., Wang, Y., Sun, Y., and McElroy, M. B.: Fine-particle pH for Beijing winter haze as inferred from different thermodynamic equilibrium models, *Atmos. Chem. Phys.*, 18, 7423-7438, <https://doi.org/10.5194/acp-18-7423-2018>, 2018.
- 835 Stauffer, D. R., and Seaman, N. L.: Use of Four-Dimensional Data Assimilation in a Limited-Area Mesoscale Model. Part I: Experiments with Synoptic-Scale Data, *Monthly Weather Review*, 118, 1250-1277, [https://doi.org/10.1175/1520-0493\(1990\)118<1250:Uofdda>2.0.Co;2](https://doi.org/10.1175/1520-0493(1990)118<1250:Uofdda>2.0.Co;2), 1990.
- Stokes, R. H., and Robinson, R. A.: Interactions in Aqueous Nonelectrolyte Solutions. I. Solute-Solvent Equilibria, *J. Phys. Chem.*, 70, 2126-2131, <https://doi.org/10.1021/j100879a010>, 1966.
- 840 Sun, Y. L., Wang, Z. F., Fu, P. Q., Jiang, Q., Yang, T., Li, J., and Ge, X. L.: The impact of relative humidity on aerosol composition and evolution processes during wintertime in Beijing, China, *Atmos. Environ.*, 77, 927-934, <https://doi.org/10.1016/j.atmosenv.2013.06.019>, 2013.

- Surratt, J. D., Lewandowski, M., Offenberg, J. H., Jaoui, M., Kleindienst, T. E., Edney, E. O., and Seinfeld, J. H.: Effect of acidity on secondary organic aerosol formation from isoprene, *Environ Sci Technol*, 41, 5363-5369, <https://doi.org/10.1021/es0704176>, 2007.
- 845 Tan, T., Hu, M., Li, M., Guo, Q., Wu, Y., Fang, X., Gu, F., Wang, Y., and Wu, Z.: New insight into PM_{2.5} pollution patterns in Beijing based on one-year measurement of chemical compositions, *Sci. Total Environ.*, 621, 734-743, <https://doi.org/10.1016/j.scitotenv.2017.11.208>, 2018.
- Tao, W., Su, H., Zheng, G., Wang, J., Wei, C., Liu, L., Ma, N., Li, M., Zhang, Q., Pöschl, U., and Cheng, Y.: Aerosol pH and chemical regimes of sulfate formation in aerosol water during winter haze in the North China Plain, *Atmos. Chem. Phys.*, 20, 11729-11746, <https://doi.org/10.5194/acp-20-11729-2020>, 2020.
- 850 Tao, Y., and Murphy, J. G.: The sensitivity of PM_{2.5} acidity to meteorological parameters and chemical composition changes: 10-year records from six Canadian monitoring sites, *Atmos. Chem. Phys.*, 19, 9309-9320, <https://doi.org/10.5194/acp-19-9309-2019>, 2019.
- 855 Tie, X., Huang, R.-J., Cao, J., Zhang, Q., Cheng, Y., Su, H., Chang, D., Pöschl, U., Hoffmann, T., Dusek, U., Li, G., Worsnop, D. R., and O'Dowd, C. D.: Severe Pollution in China Amplified by Atmospheric Moisture, *Scientific Reports*, 7, 15760, <https://doi.org/10.1038/s41598-017-15909-1>, 2017.
- Tilgner, A., Schaefer, T., Alexander, B., Barth, M., Collett, J. L., Fahey, K. M., Nenes, A., Pye, H. O. T., Herrmann, H., and McNeill, V. F.: Acidity and the multiphase chemistry of atmospheric aqueous particles and clouds, *Atmos. Chem. Phys.*, 21, 13483-13536, <https://doi.org/10.5194/acp-21-13483-2021>, 2021.
- 860 Vasilakos, P., Russell, A., Weber, R., and Nenes, A.: Understanding nitrate formation in a world with less sulfate, *Atmos. Chem. Phys.*, 18, 12765-12775, <https://doi.org/10.5194/acp-18-12765-2018>, 2018.
- 865 Wang, G., Zhang, R., Gomez, M. E., Yang, L., Levy Zamora, M., Hu, M., Lin, Y., Peng, J., Guo, S., Meng, J., Li, J., Cheng, C., Hu, T., Ren, Y., Wang, Y., Gao, J., Cao, J., An, Z., Zhou, W., Li, G., Wang, J., Tian, P., Marrero-Ortiz, W., Secretst, J., Du, Z., Zheng, J., Shang, D., Zeng, L., Shao, M., Wang, W., Huang, Y., Wang, Y., Zhu, Y., Li, Y., Hu, J., Pan, B., Cai, L., Cheng, Y., Ji, Y., Zhang, F., Rosenfeld, D., Liss, P. S., Duce, R. A., Kolb, C. E., and Molina, M. J.: Persistent sulfate formation from London Fog to Chinese haze, *Proc. Natl. Acad. Sci. U. S. A.*, 113, 13630-13635, <https://doi.org/10.1073/pnas.1616540113>, 2016.
- 870 Wang, H. Y., Zhang, D., Zhang, Y. T., Zhai, L. M., Yin, B., Zhou, F., Geng, Y. C., Pan, J. T., Luo, J. F., Gu, B. J., and Liu, H. B.: Ammonia emissions from paddy fields are underestimated in China, *Environ. Pollut.*, 235, 482-488, <https://doi.org/10.1016/j.envpol.2017.12.103>, 2018.
- 875 Wang, S. B., Wang, L. L., Li, Y. Q., Wang, C., Wang, W. S., Yin, S. S., and Zhang, R. Q.: Effect of ammonia on fine-particle pH in agricultural regions of China: comparison between urban and rural sites, *Atmos. Chem. Phys.*, 20, 2719-2734, <https://doi.org/10.5194/acp-20-2719-2020>, 2020a.
- Wang, W., Liu, M., Wang, T., Song, Y., Zhou, L., Cao, J., Hu, J., Tang, G., Chen, Z., Li, Z., Xu, Z., Peng, C., Lian, C., Chen, Y., Pan, Y., Zhang, Y., Sun, Y., Li, W., Zhu, T., Tian, H., and Ge, M.: Sulfate formation is dominated by manganese-catalyzed oxidation of SO₂ on aerosol surfaces during haze events, *Nat. Commun.*, 12, 1993, <https://doi.org/10.1038/s41467-021-22091-6>, 2021.
- 880 Wang, X., Jacob, D. J., Eastham, S. D., Sulprizio, M. P., Zhu, L., Chen, Q., Alexander, B., Sherwen, T., Evans, M. J., Lee, B. H., Haskins, J. D., Lopez-Hilfiker, F. D., Thornton, J. A., Huey, G. L., and Liao,

- H.: The role of chlorine in global tropospheric chemistry, *Atmos. Chem. Phys.*, 19, 3981-4003, <https://doi.org/10.5194/acp-19-3981-2019>, 2019.
- 885 Wang, X., Jacob, D. J., Fu, X., Wang, T., Breton, M. L., Hallquist, M., Liu, Z., McDuffie, E. E., and Liao, H.: Effects of Anthropogenic Chlorine on PM_{2.5} and Ozone Air Quality in China, *Environ. Sci. Technol.*, 54, 9908-9916, <https://doi.org/10.1021/acs.est.0c02296>, 2020b.
- Weber, R. J., Guo, H. Y., Russell, A. G., and Nenes, A.: High aerosol acidity despite declining atmospheric sulfate concentrations over the past 15 years, *Nat. Geosci.*, 9, 282-285, <https://doi.org/10.1038/Ngeo2665>, 2016.
- 890 Wu, Z., Wang, Y., Tan, T., Zhu, Y., Li, M., Shang, D., Wang, H., Lu, K., Guo, S., Zeng, L., and Zhang, Y.: Aerosol Liquid Water Driven by Anthropogenic Inorganic Salts: Implying Its Key Role in Haze Formation over the North China Plain, *Environ. Sci. Technol. Lett.*, 5, 160-166, <https://doi.org/10.1021/acs.estlett.8b00021>, 2018.
- Xie, Y., Wang, G., Wang, X., Chen, J., Chen, Y., Tang, G., Wang, L., Ge, S., Xue, G., Wang, Y., and 895 Gao, J.: Nitrate-dominated PM_{2.5} and elevation of particle pH observed in urban Beijing during the winter of 2017, *Atmos. Chem. Phys.*, 20, 5019-5033, <https://doi.org/10.5194/acp-20-5019-2020>, 2020.
- Yang, W., Zhang, Y., Wang, X., Li, S., Zhu, M., Yu, Q., Li, G., Huang, Z., Zhang, H., Wu, Z., Song, W., Tan, J., and Shao, M.: Volatile organic compounds at a rural site in Beijing: influence of temporary 900 emission control and wintertime heating, *Atmos. Chem. Phys.*, 18, 12663-12682, <https://doi.org/10.5194/acp-18-12663-2018>, 2018.
- Zaveri, R. A., and Peters, L. K.: A new lumped structure photochemical mechanism for large-scale applications, *J. Geophys. Res.-Atmos.*, 104, 30387-30415, <https://doi.org/10.1029/1999jd900876>, 1999.
- Zaveri, R. A., Easter, R. C., and Peters, L. K.: A computationally efficient multicomponent equilibrium 905 solver for aerosols (MESA), *J. Geophys. Res.-Atmos.*, 110, <https://doi.org/10.1029/2004JD005618>, 2005a.
- Zaveri, R. A., Easter, R. C., and Wexler, A. S.: A new method for multicomponent activity coefficients of electrolytes in aqueous atmospheric aerosols, *J. Geophys. Res.-Atmos.*, 110, D02201, <https://doi.org/10.1029/2004jd004681>, 2005b.
- 910 Zaveri, R. A., Easter, R. C., Fast, J. D., and Peters, L. K.: Model for Simulating Aerosol Interactions and Chemistry (MOSAIC), *J. Geophys. Res.-Atmos.*, 113, <https://doi.org/10.1029/2007JD008782>, 2008.
- Zdanovskii, A.: New methods for calculating solubilities of electrolytes in multicomponent systems, *Zh. Fiz. Khim.*, 22, 1475-1485, 1948.
- Zhang, B., Shen, H., Liu, P., Guo, H., Hu, Y., Chen, Y., Xie, S., Xi, Z., Skipper, T. N., and Russell, A. 915 G.: Significant contrasts in aerosol acidity between China and the United States, *Atmos. Chem. Phys.*, 21, 8341-8356, <https://doi.org/10.5194/acp-21-8341-2021>, 2021.
- Zhang, J., Chen, Z., Lu, Y., Gui, H., Liu, J., Liu, W., Wang, J., Yu, T., Cheng, Y., Chen, Y., Ge, B., Fan, Y., and Luo, X.: Characteristics of aerosol size distribution and vertical backscattering coefficient profile during 2014 APEC in Beijing, *Atmos. Environ.*, 148, 30-41, 920 <https://doi.org/10.1016/j.atmosenv.2016.10.020>, 2017.

- Zhang, L., Chen, Y. F., Zhao, Y. H., Henze, D. K., Zhu, L. Y., Song, Y., Paulot, F., Liu, X. J., Pan, Y. P., Lin, Y., and Huang, B. X.: Agricultural ammonia emissions in China: reconciling bottom-up and top-down estimates, *Atmos. Chem. Phys.*, 18, 339-355, <https://doi.org/10.5194/acp-18-339-2018>, 2018.
- 925 Zhao, C., Liu, X., Leung, L. R., Johnson, B., McFarlane, S. A., Gustafson Jr, W. I., Fast, J. D., and Easter, R.: The spatial distribution of mineral dust and its shortwave radiative forcing over North Africa: modeling sensitivities to dust emissions and aerosol size treatments, *Atmos. Chem. Phys.*, 10, 8821-8838, <https://doi.org/10.5194/acp-10-8821-2010>, 2010.
- 930 Zhao, C., Chen, S., Leung, L. R., Qian, Y., Kok, J. F., Zaveri, R. A., and Huang, J.: Uncertainty in modeling dust mass balance and radiative forcing from size parameterization, *Atmos. Chem. Phys.*, 13, 10733-10753, <https://doi.org/10.5194/acp-13-10733-2013>, 2013a.
- Zhao, C., Leung, L. R., Easter, R., Hand, J., and Avise, J.: Characterization of speciated aerosol direct radiative forcing over California, *J. Geophys. Res.-Atmos.*, 118, 2372-2388, <https://doi.org/10.1029/2012jd018364>, 2013b.
- 935 Zheng, G., Su, H., Wang, S., Andreae, M. O., Poschl, U., and Cheng, Y.: Multiphase buffer theory explains contrasts in atmospheric aerosol acidity, *Science*, 369, 1374-1377, <https://doi.org/10.1126/science.aba3719>, 2020.

940

|

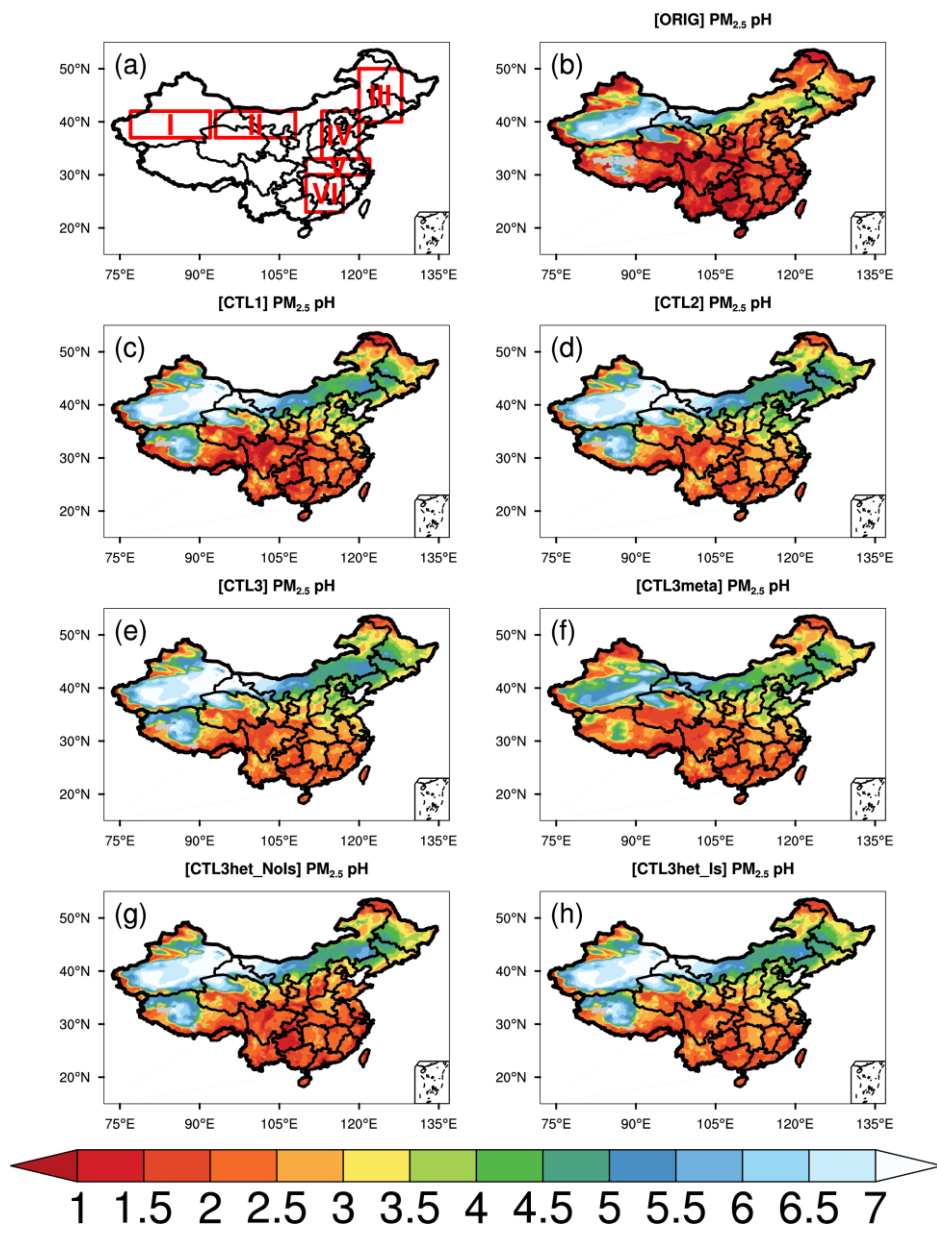
Table 1. Summary of model configurations.

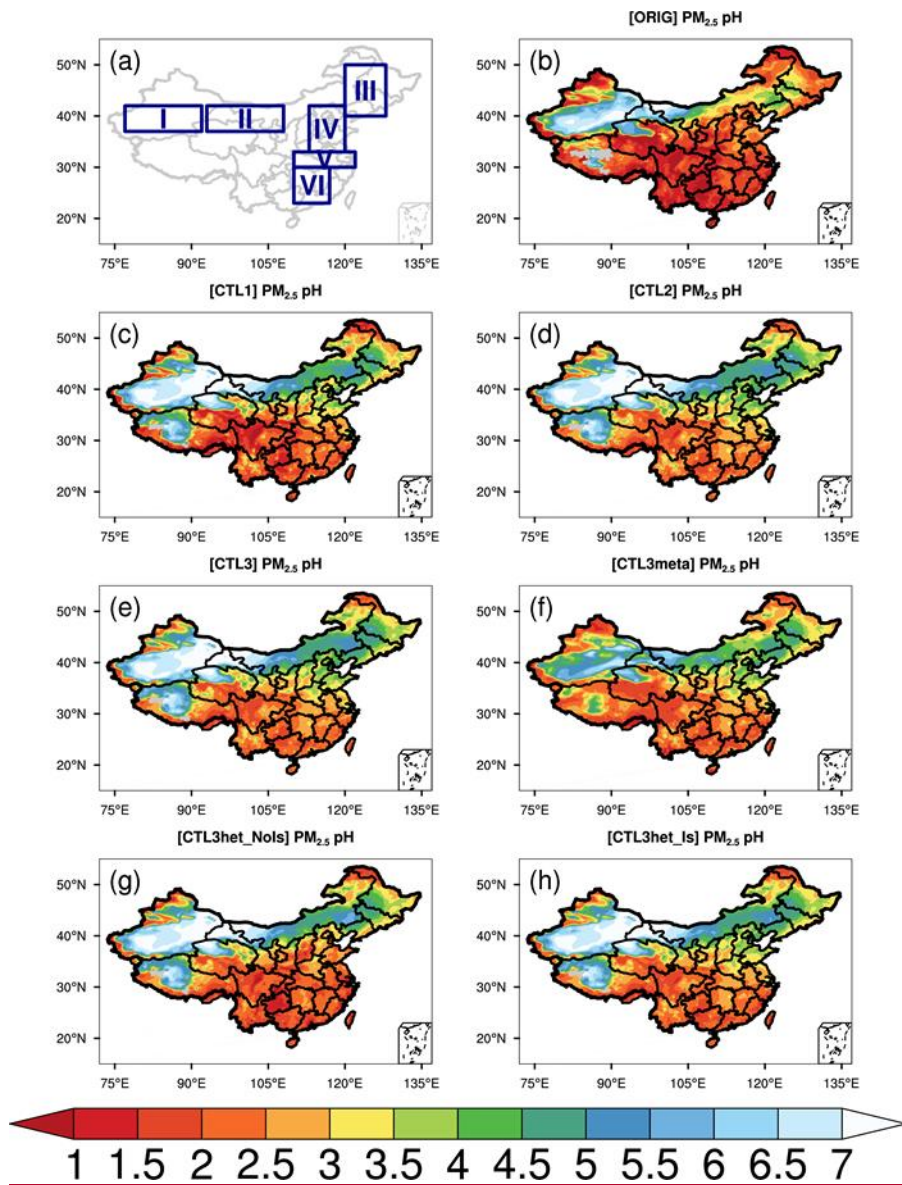
Description	Selection
Horizontal grid spacing	36 km
<u>Vertical levels</u>	<u>41 (roughly 8 layers below 1 km)</u>
Grid dimensions	149 × 138
Aerosol scheme	MOSAIC 8 bin
Gas-phase chemistry	CBM-Z
Long wave Radiation	RRTMG
Short wave Radiation	RRTMG
Cloud Microphysics	Morrison 2-moment
Cumulus Cloud	Grell-Devenyi
Planetary boundary layer	YSU
Land surface	Noah land-surface model
<u>Nudging variables</u>	<u>u and v component wind, air temperature, water vapor mixing ratio</u>
<u>Grid nudging Applied layers</u>	<u>Layers above the PBL</u>
<u>Nudging timescale</u>	<u>6 h</u>

945 **Table 2.** Numerical experiments conducted in this study.

Name	Cation	NH₃ emission	Cl emission	Phase state	Sulfate production
ORIG	default	default	default	default ^a	default
CTL1	modify	default	default	default	default
CTL2	modify	×2	default	default	default
CTL3	modify	×2	modify	default	default
CTL3meta	modify	×2	modify	metastable	default
CTL3het_NoIs	modify	×2	modify	default	Add het (No Is effect)
CTL3het_Is	modify	×2	modify	default	Add het (consider Is effect)

^aBy default, in MOSAIC a flag called “hysteresis water content” (W_{hyst}) is transported to determine whether the particles are on the stable or the metastable branch.

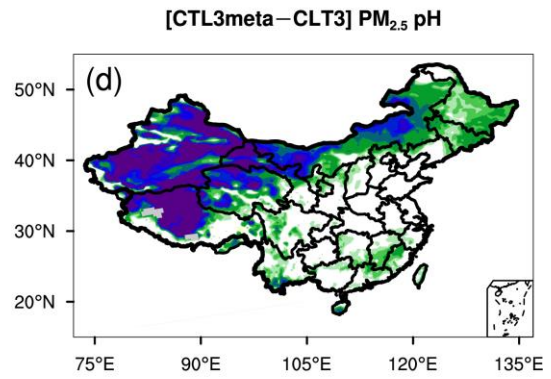
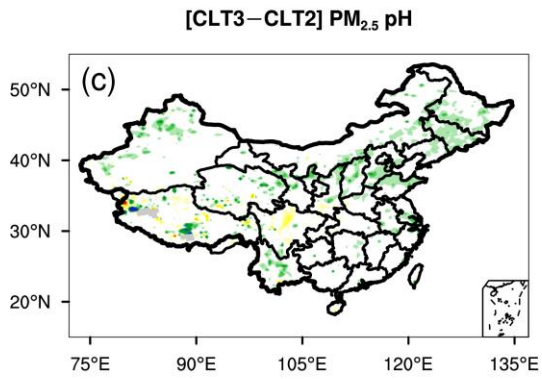
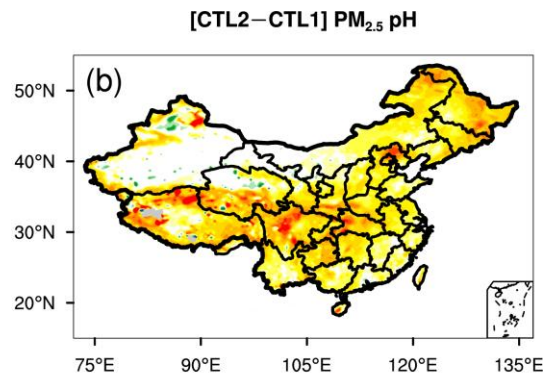
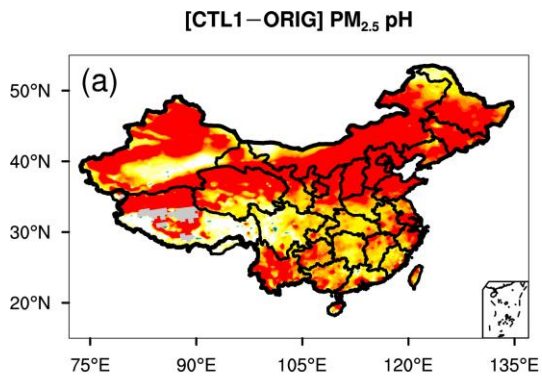




950

Figure 1. (a) Six sub-regions. (b-h) Spatial distributions of mean surface PM_{2.5} pH (LWC-weighted average pH) during the study period of 15 October 2014 - 02 November 2014 predicted by (b) ORIG (c) CTL1 (d) CTL2 (e) CTL3 (f) CTL3meta (g) CTL3het_NoIs (h) CTL3het_Is. “I” in (a) represents the Taklimakan Desert (TD), “II” represents the Gobi Desert (GD), “III” represents the Northeast Plain (NEP), “IV” represents the North China Plain (NCP), “V” represents the middle and lower reaches of Yangtze River plain (YR), and “VI” represents Southern China (SC).

955



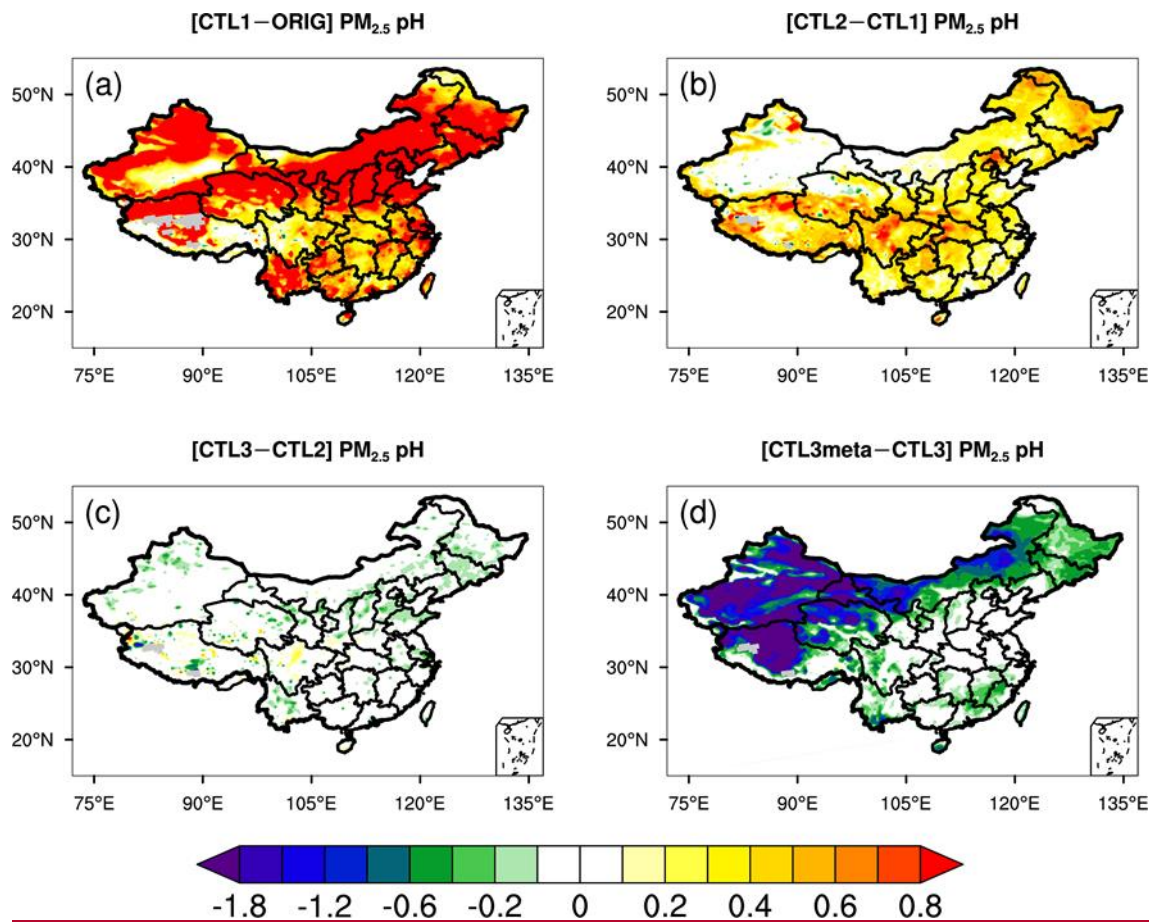
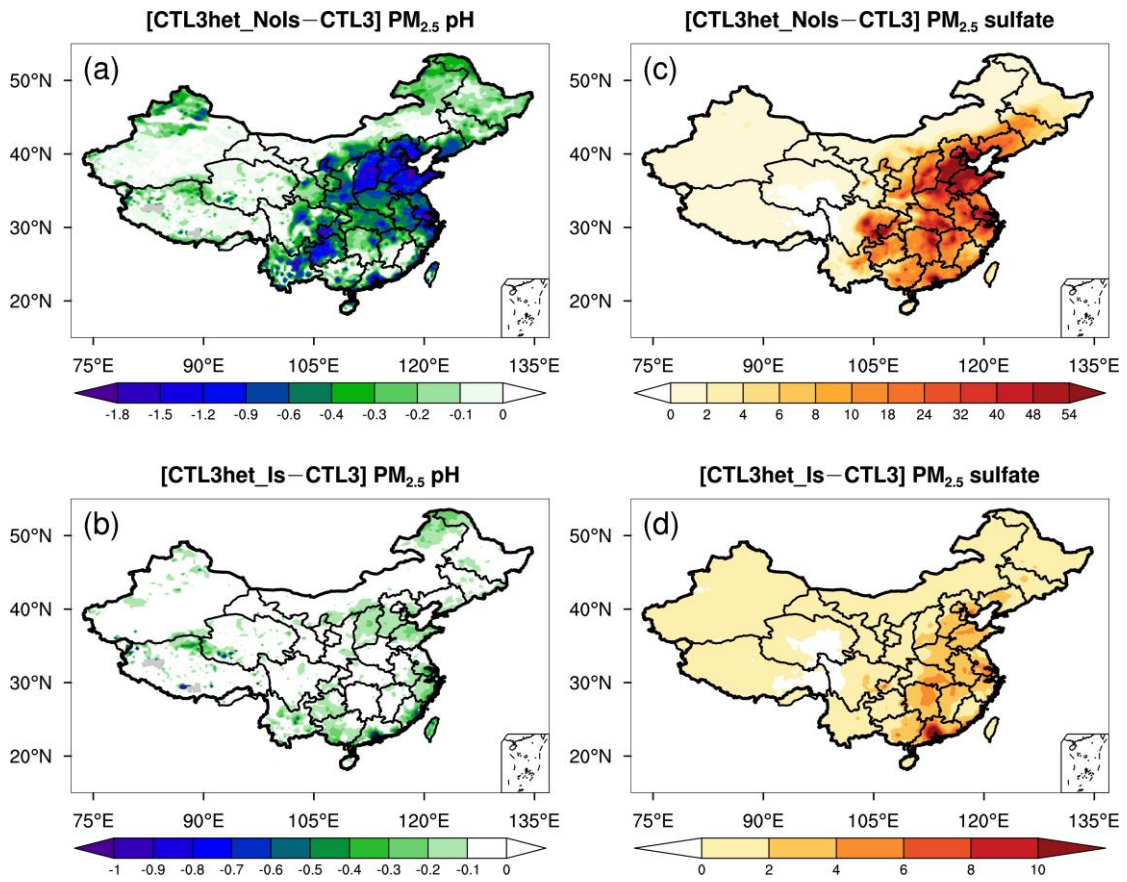


Figure 2. Spatial distributions of the difference in mean surface PM_{2.5} pH during the study period of 15 October 2014 - 02 November 2014 between (a) ~~CTL1~~ and ORIG scenarios, (b) CTL2 and CTL1 scenarios, (c) CTL3 and CTL2 scenarios, (d) CTL3meta and CTL3 scenarios.

960

965

970



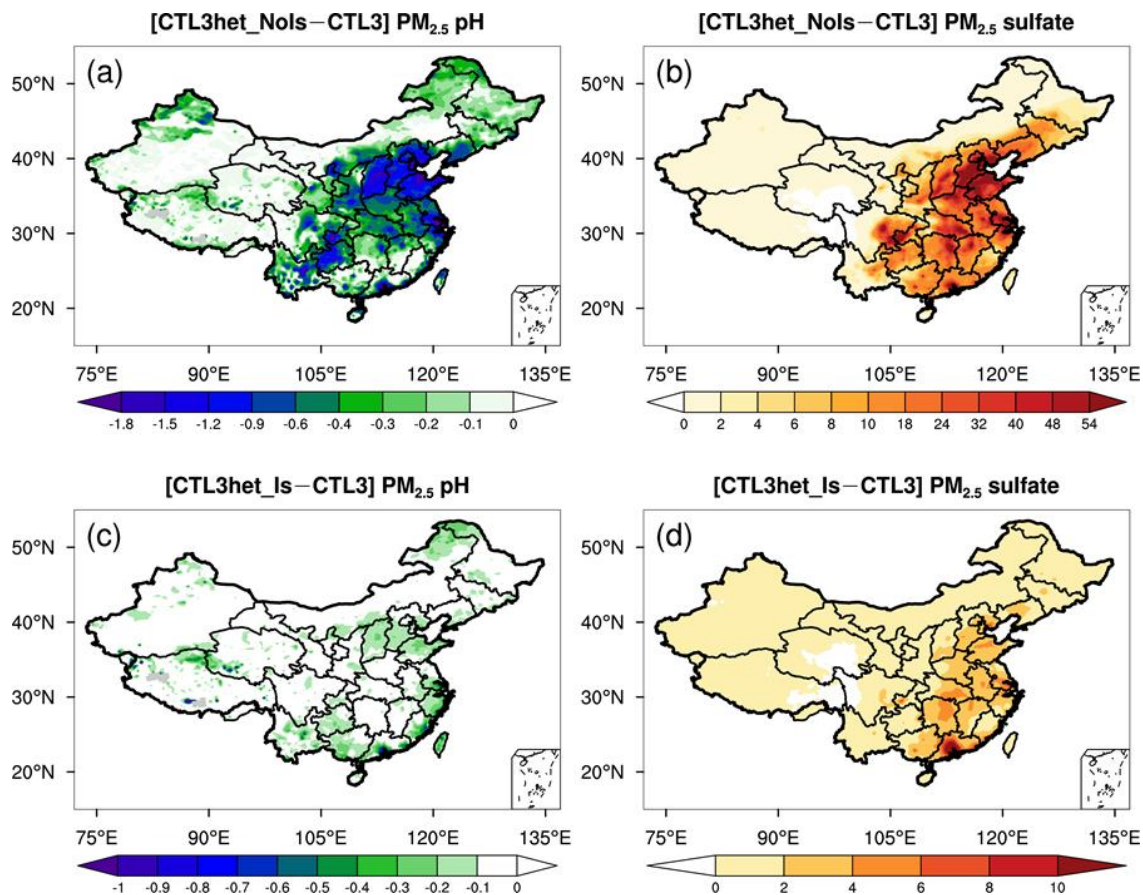


Figure 3. Spatial distributions of the difference in mean surface (a,c) $PM_{2.5}$ pH and (b,d) $PM_{2.5}$ sulfate ($\mu g m^{-3}$) between (top panels) CTL3het_NoIs and CTL3 scenarios (top panels), and (bottom panels) CTL3het_Is and CTL3 scenarios (bottom panels) during the study period of 15 October 2014 - 02 November 2014. Different scales are used.

975

980

985

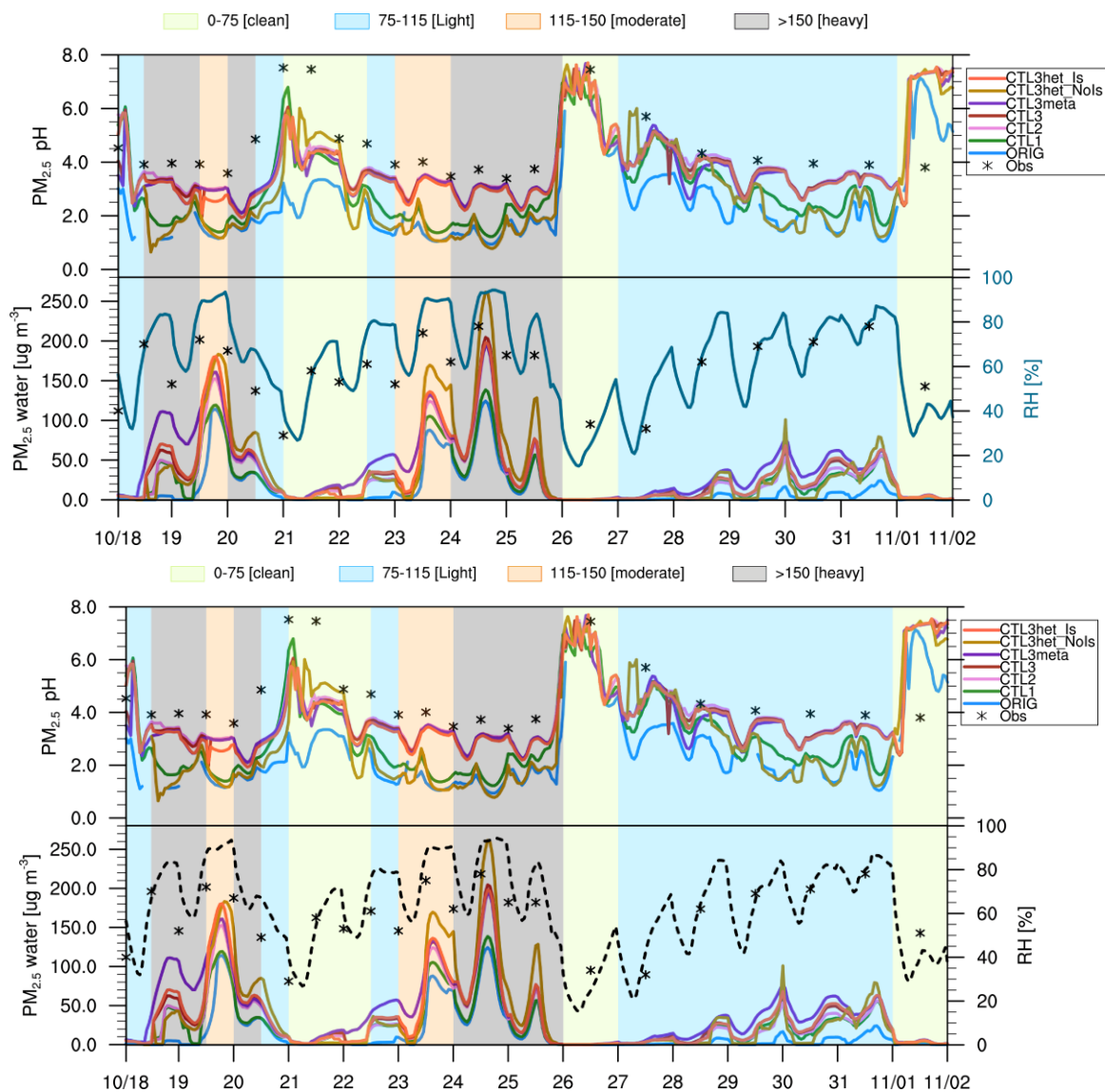
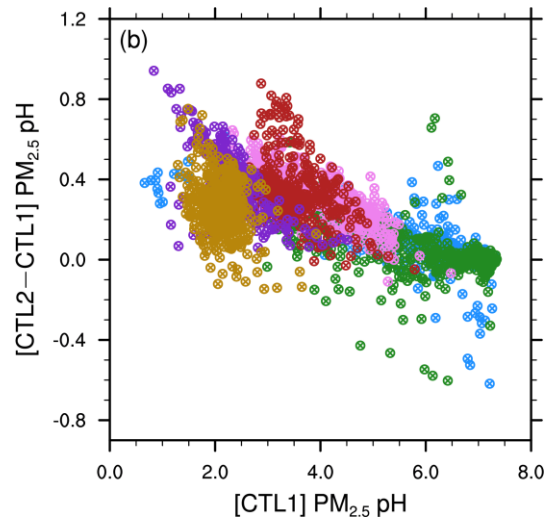
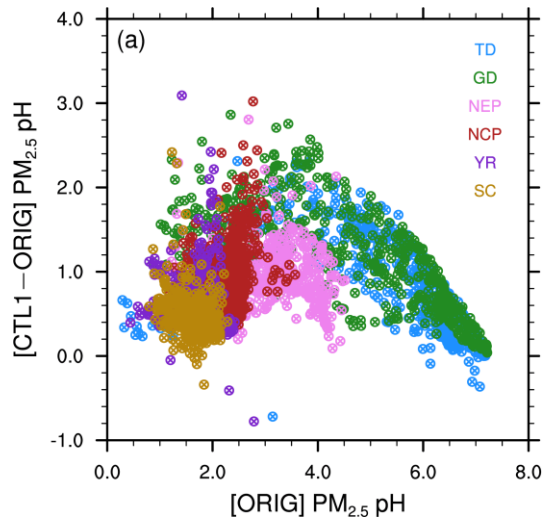


Figure 4. Time series of (top panel) surface $PM_{2.5}$ pH, and (bottom panel) $PM_{2.5}$ water contents ($\mu\text{g m}^{-3}$) (left y-axis) predicted by all WRF-Chem scenarios at Beijing site during the study period of 15 October 2014 - 02 November 2014 and Relative humidity (%) (RH, right y-axis, black dashed line) are given from ORIG scenario. ISORROPIA II-calculated pH values constrained by observations as well as the observed RH are shown as black star markers, with each value corresponding to a $PM_{2.5}$ sample (12h or 24h). Shaded areas represent four different pollution levels (green-clean; blue-light; orange-moderate; grey-heavy).



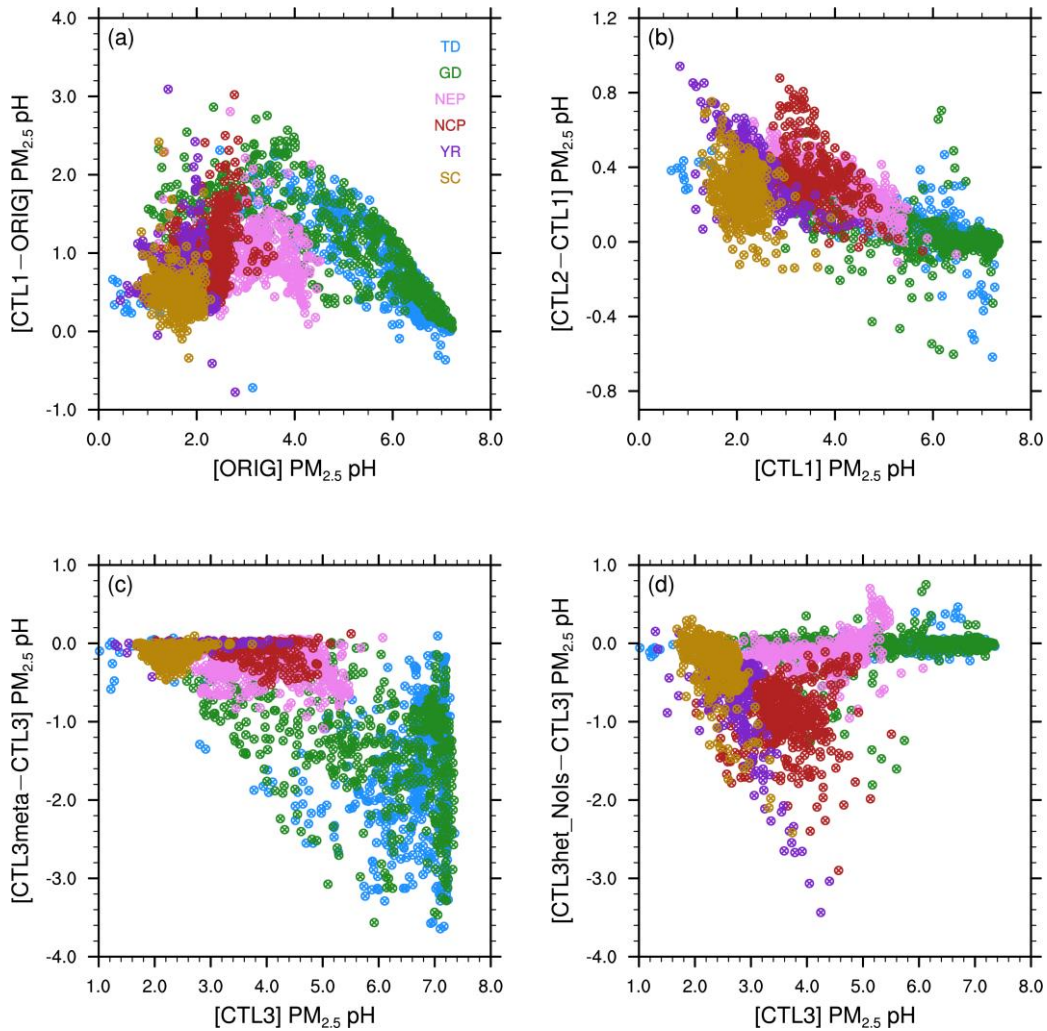


Figure 5. Scatterplots of the surface $PM_{2.5}$ pH differences between (a) ~~CTL~~CTL1 and ORIG scenarios, (b) CTL2 and CTL1 scenarios, (c) CTL3meta and CTL3 scenarios, (d) CTL3het_NoIs and CTL3 scenarios vs. the corresponding original pH, separated by regions. Different scales are used.

1000

1005

1010

1015

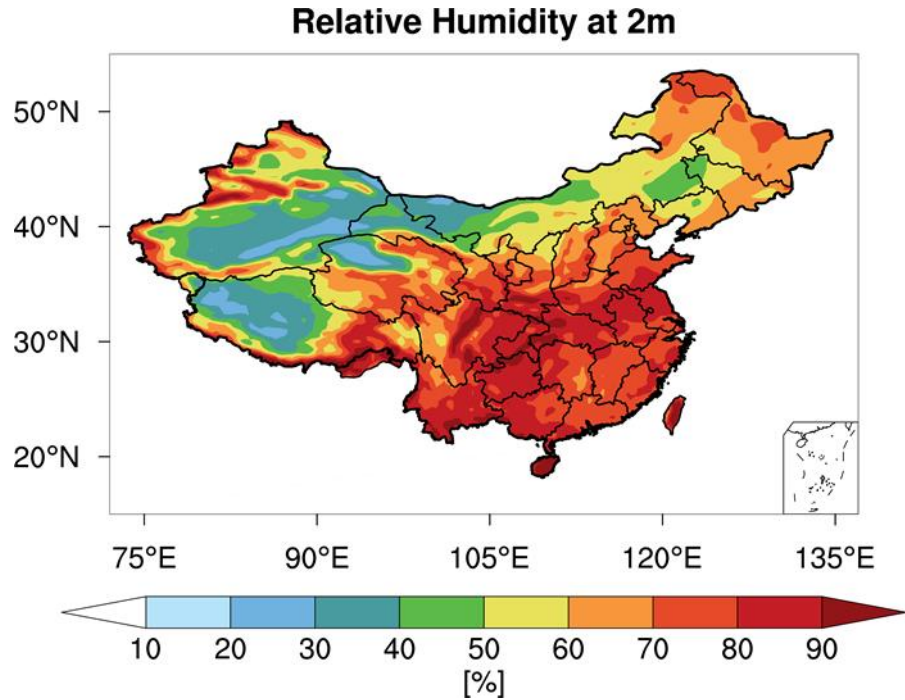


Figure 6. Spatial distribution of mean 2m relative humidity [%] from WRF-Chem during the study period of 15 October 2014 - 02 November 2014.

1020

1025

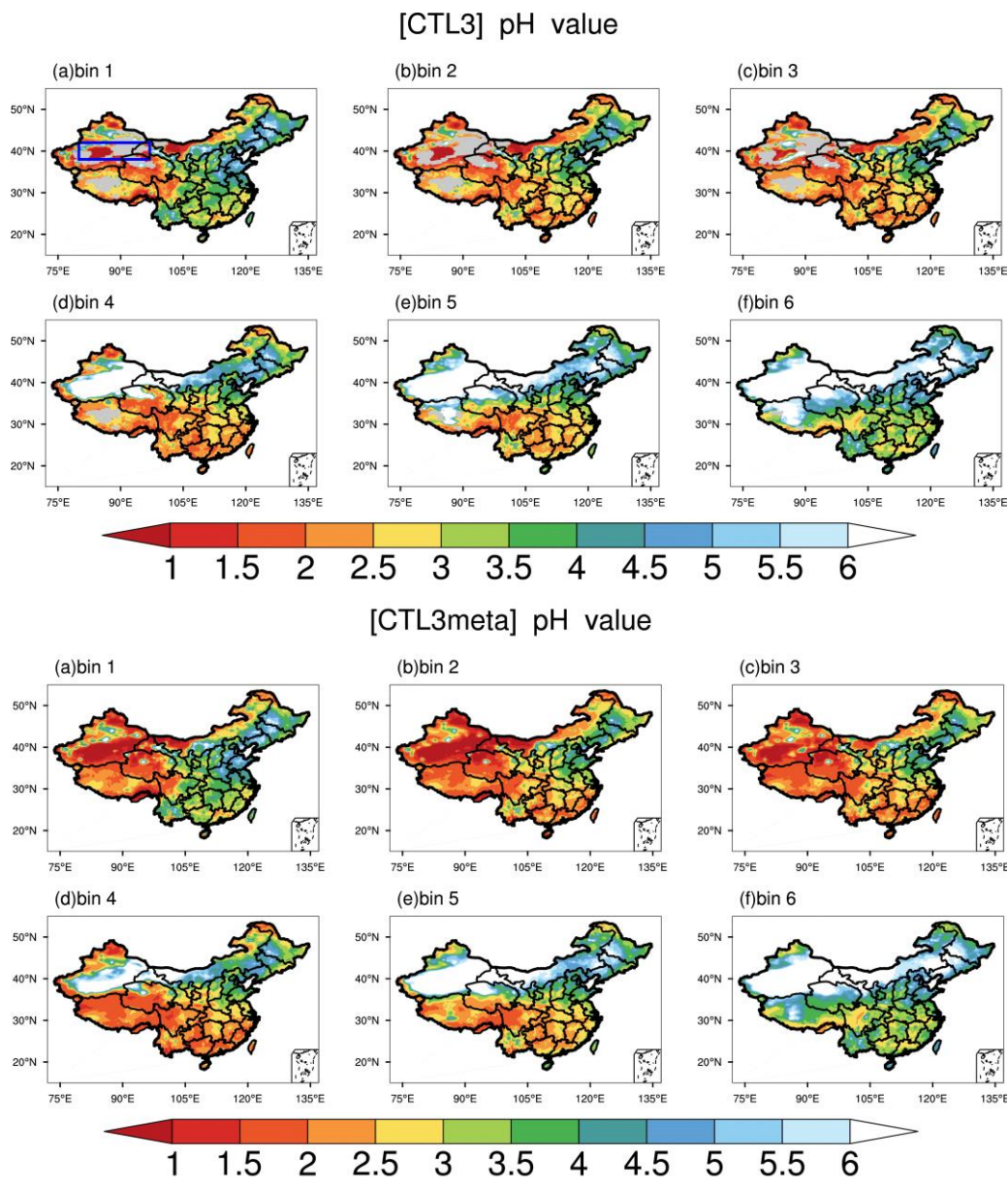


Figure 7. Spatial distributions of mean surface aerosol pH during the study period of 15 October 2014 - 02 November 2014 predicted by (top panel) CTL3 scenario and (bottom panel) CTL3meta scenario for six size bins. (a) Bin 1 for 0.039-0.078 μm diameter, (b) Bin 2 for 0.078-0.156 μm diameter, (c) Bin 3 for 0.156-0.312 μm diameter, (d) Bin 4 for 0.312-0.625 μm diameter, (e) Bin 5 for 0.625-1.25 μm diameter, (f) Bin 6 for 1.25-2.5 μm diameter. The blue box in top panel (a) represents the focus area of analysis in follow.

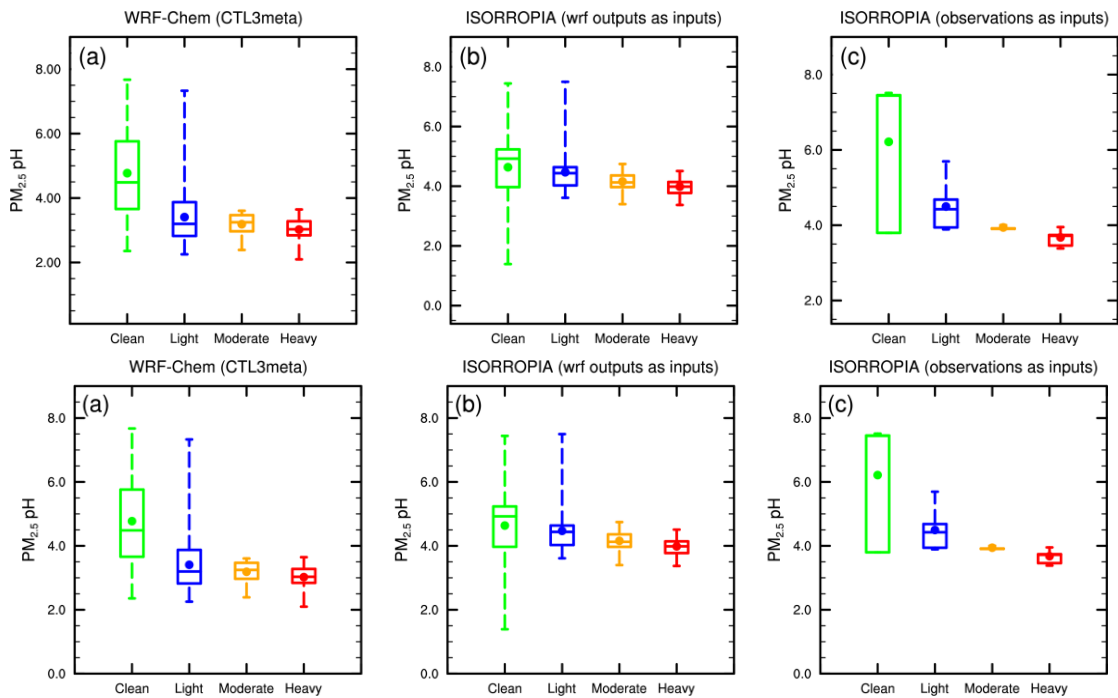


Figure 86. The box-and-whisker plots of surface $PM_{2.5}$ pH in each haze stage in Beijing from (a) WRF-Chem CTL3meta scenario, (b) ISORROPIA predictions with WRF-Chem (CTL3meta) relevant outputs as inputs, and (c) ISORROPIA predictions with observations as inputs. The boxes represent, from top to bottom, the 75th, 50th, and 25th percentiles of statistical data. The whiskers represent, from top to bottom, the minimum and the maximum, and the solid circles represent the mean values.

1040

1045

1050

1055

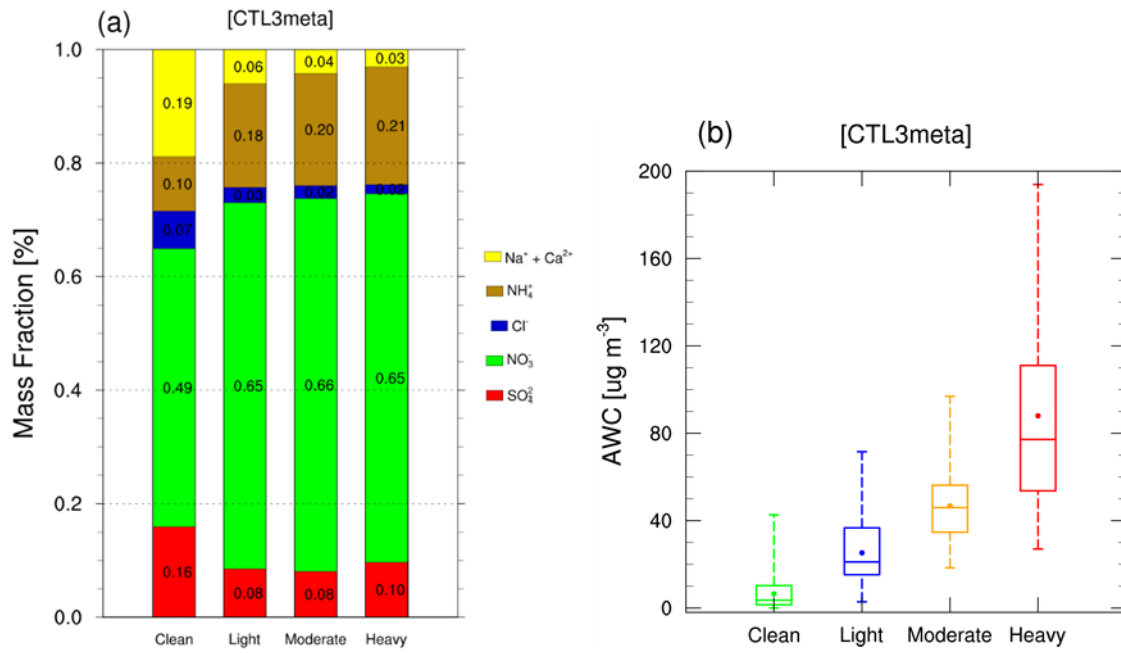


Figure 9. Modeled (a) mass fractions [%] of PM_{2.5} ionic species and (b) AWC (µg m⁻³) from CTL3meta scenario in each haze stage.

1060

1065

1070

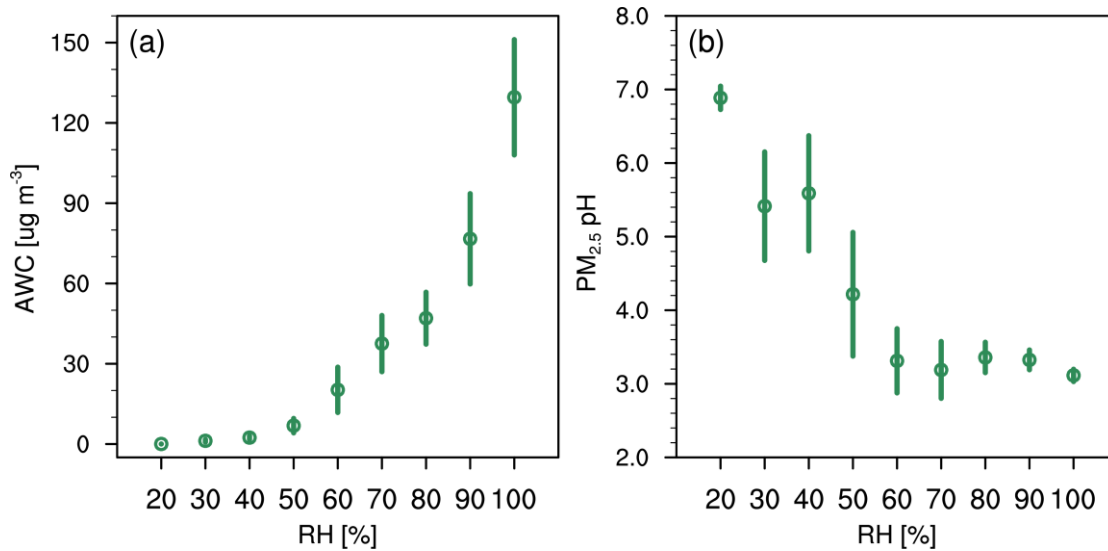


Figure 107. (a) AWC ($\mu\text{g m}^{-3}$) and (b) PM_{2.5} pH predicted by CTL3meta scenario as a function of RH for data at Beijing site during the study period of 15 October 2014 - 02 November 2014. Data are grouped in RH bins (10% increment). The error bars represent the standard deviations.

1075

1080

1085

1090

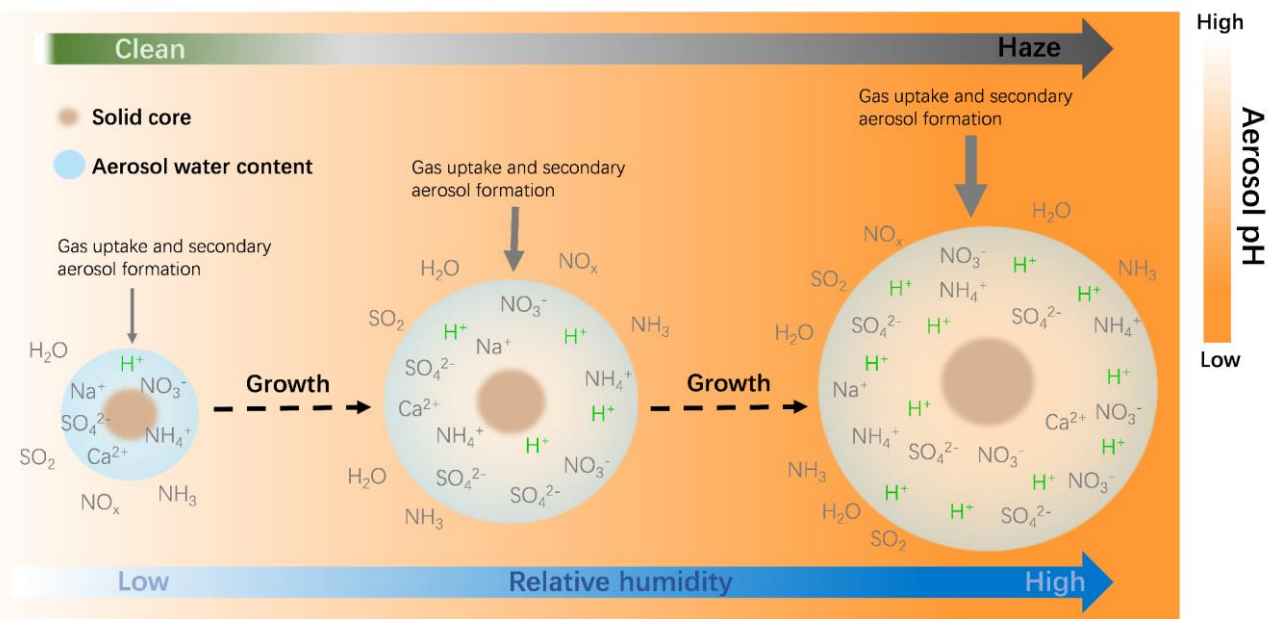


Figure 11. The schematic plot of the temporal evolution of $PM_{2.5}$ pH during haze cycle in Beijing. The size of blue circles indicates the relative amount of aerosol water and the thickness of downward arrows indicates the relative strength of the process.